Neuron

NeuroResource

Wireless Optogenetic Stimulation of Oxytocin Neurons in a Semi-natural Setup Dynamically Elevates Both Pro-social and Agonistic Behaviors

Graphical Abstract

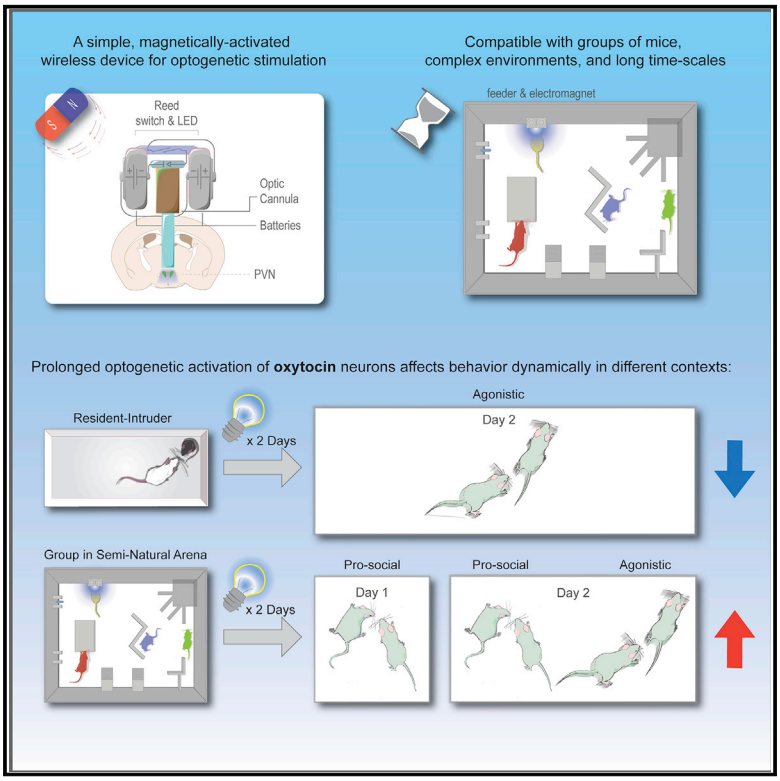

Highlights

- A small, wireless device is used for optogenetic activation in a complex environment
- PVN oxytocin neurons were activated repeatedly over 2 days in a group setting
- Repeated activation in a group setting elicited both pro-social and agonistic behavior
- Findings support the social salience hypothesis of oxytocin neuro-modulation

Authors

Sergey Anpilov, Yair Shemesh, Noa Eren, ..., Shlomo Wagner, Ofer Yizhar, Alon Chen

Correspondence

alon.chen@weizmann.ac.il

In Brief

Anpilov et al. present a lightweight, easily assembled wireless optogenetic device compatible with group-housed mice in a complex environment. Using this approach, they show that repeated activation of oxytocin neurons elicits both pro-social and aggressive behaviors over time, emphasizing the role of the social setting in modulating behavior.

Anpilov et al., 2020, Neuron *107*, 1–12
August 19, 2020
https://doi.org/10.1016/j.neuron.2020.05.028

CellPress

Neuron

CellPress
OPEN ACCESS

NeuroResource

Wireless Optogenetic Stimulation of Oxytocin Neurons in a Semi-natural Setup Dynamically Elevates Both Pro-social and Agonistic Behaviors

Sergey Anpilov,[1,2,5] Yair Shemesh,[1,2,5] Noa Eren,[1,2,5] Hala Harony-Nicolas,[3] Asaf Benjamin,[1,2] Julien Dine,[1,2] Vinícius E.M. Oliveira,[4] Oren Forkosh,[1,2] Stoyo Karamihalev,[1,2] Rosa-Eva Hüttl,[1,2] Noa Feldman,[1] Ryan Berger,[1] Avi Dagan,[1] Gal Chen,[1] Inga D. Neumann,[4] Shlomo Wagner,[3] Ofer Yizhar,[1] and Alon Chen[1,2,6,*]

[1]Department of Neurobiology, Weizmann Institute of Science, Rehovot 7610001, Israel
[2]Department of Stress Neurobiology and Neurogenetics, Max Planck Institute of Psychiatry, Munich 80804, Germany
[3]Sagol Department of Neurobiology, University of Haifa, Haifa 3498838, Israel
[4]Department of Behavioural and Molecular Neurobiology, Regensburg Center of Neuroscience, University of Regensburg, Regensburg 93053, Germany
[5]These authors contributed equally
[6]Lead Contact
*Correspondence: alon.chen@weizmann.ac.il
https://doi.org/10.1016/j.neuron.2020.05.028

SUMMARY

Complex behavioral phenotyping techniques are becoming more prevalent in the field of behavioral neuroscience, and thus methods for manipulating neuronal activity must be adapted to fit into such paradigms. Here, we present a head-mounted, magnetically activated device for wireless optogenetic manipulation that is compact, simple to construct, and suitable for use in group-living mice in an enriched semi-natural arena over several days. Using this device, we demonstrate that repeated activation of oxytocin neurons in male mice can have different effects on pro-social and agonistic behaviors, depending on the social context. Our findings support the social salience hypothesis of oxytocin and emphasize the importance of the environment in the study of social neuromodulators. Our wireless optogenetic device can be easily adapted for use in a variety of behavioral paradigms, which are normally hindered by tethered light delivery or a limited environment.

INTRODUCTION

The field of behavioral neuroscience is undergoing a transformation in terms of the methodology of behavioral phenotyping, with an emphasis on measuring behavior in more ethologically relevant conditions. Standardized and often reductionist methods, which have been widely used to assess animal behavior, have given rise to most of the current scientific knowledge in the field. Yet, especially in the domain of social behavior, researchers have raised concern regarding studies that rely merely on restricted assays in simplified environments, which may not accurately reflect rich and diverse behavioral repertoires (Kondrakiewicz et al., 2019; Peters et al., 2015; Zilkha et al., 2016).

In an aim to address this concern, we previously developed an experimental system that allows animals to behave freely in a large environment, enriched with hiding places, elevated platforms, bedding, feeders, and water sources, while their location is tracked automatically over days, and dozens of behavioral readouts are extracted (Forkosh et al., 2019; Shemesh et al., 2013, 2016).

In order to study the impact of neural circuit manipulations on complex, unrestrained social behavior, we aimed to incorporate optogenetics into our system. However, semi-natural setups for measuring behavior are incompatible with traditional optogenetic approaches, which use tethered light delivery systems. The main challenges of incorporating wireless optogenetics technology in semi-natural setups are to remotely control a compact and lightweight device, that will produce a strong enough light intensity to activate a given opsin in any brain region. On top of that, and most importantly, the system must be suitable for operation in large, enriched, and versatile environments that include all kinds of materials and parts.

Current wireless optogenetic technologies are based on specific light wavelengths delivered from light-emitting diodes (LEDs). Some of them employ external LEDs, which are either directly adjacent to superficial target areas (Wentz et al., 2011) or are combined with optic fibers to conduct light into deeper regions (Dagnew et al., 2017; Emara et al., 2018; Gagnon-Turcotte et al., 2019). Others make use of ultra-miniature LEDs, which can be injected directly into the target tissue (Jeong et al., 2015; Kim et al., 2013; Mickle et al., 2019; Montgomery et al., 2015; Park et al., 2015b, 2015a; Qazi et al., 2019; Rossi et al., 2015; Shin et al., 2017). The power supply can be based on a replaceable power source carried on the animal's body (Dagnew

Please cite this article in press as: Anpilov et al., Wireless Optogenetic Stimulation of Oxytocin Neurons in a Semi-natural Setup Dynamically Elevates Both Pro-social and Agonistic Behaviors, Neuron (2020), https://doi.org/10.1016/j.neuron.2020.05.028

et al., 2017; Gagnon-Turcotte et al., 2019; Jeong et al., 2015; Rossi et al., 2015) or a remotely chargeable power source using antennas that surround the home cage (Emara et al., 2018; Ho et al., 2014; Mickle et al., 2019; Montgomery et al., 2015; Park et al., 2015b, 2015a; Qazi et al., 2019; Shin et al., 2017; Wentz et al., 2011). While these developments are promising, none have yet, to our knowledge, been utilized in a semi-natural setup that requires durable and easy-to-handle devices, in a large and enriched environment.

Here, we present a magnetically controlled, head-mountable wireless optogenetic apparatus that is affordable, easily assembled, and implemented for prolonged manipulation of freely behaving, group-housed mice in a semi-natural arena.

To test this tool, we chose to target neurons expressing oxytocin (OT) in the paraventricular hypothalamic nucleus (PVN). OT has long been known to be involved in social behaviors and is recently being explored as a therapeutic candidate for autism spectrum disorders (ASDs) (Jurek and Neumann, 2018; Ooi et al., 2017). However, the traditional notion of OT as a potent mammalian pro-social agent largely relies on reductive paradigms such as the 3-chamber and resident-intruder (RI) assays (Lee et al., 2009). Additionally, more recent studies have demonstrated some antisocial effects of OT in both humans (De Dreu et al., 2010, 2011; Eckstein et al., 2014; Shamay-Tsoory et al., 2009) and other animals (Duque-Wilckens et al., 2018; Guzmán et al., 2013; Huang et al., 2014). These findings gave rise to the social salience hypothesis, which suggests that OT acts to regulate the salience of external social cues, rather than strictly promoting affiliative behaviors (Shamay-Tsoory and Abu-Akel, 2016; Steinman et al., 2019). Support for this idea was recently shown in a mouse study demonstrating a crucial role for OT in discriminating emotion of both positive and negative valence in a conspecific (Ferretti et al., 2019). Thus, an investigation of the prolonged behavioral effects of OT in an ethologically relevant social context could contribute to the understanding of the complex role of OT in social behavior.

Combining the use of wireless optogenetic devices with an enriched social setting, we found dynamic behavioral effects of repeated optogenetic activation of PVN-OT neurons in groups of male mice. Following an initial phase of increased social interest, which can be interpreted as pro-social behavior, we observed a concomitant increase in agonistic behavior. Surprisingly, the same prolonged activation regime robustly inhibited aggressive behavior in the RI paradigm, demonstrating that the effects of OT can be highly context dependent. These findings emphasize the importance of the social context, and of investigating a rich and diverse set of complex behavioral readouts, in the study of socially relevant neuromodulators.

RESULTS

A Wireless Device for Prolonged Optogenetic Manipulation in a Semi-natural Arena

Our device is aimed for prolonged manipulation of neuronal activity in freely behaving groups of mice in a semi-natural environment. It is small (<1 cm^3, approximately 1.5 g with dental cement coating) and head mountable and comprises a fiber optic cannula, an LED powered by two "multi-drain" watch batteries, and a magnetic field-dependent reed-switch (Figures 1A and 1B). All parts of the device are commercially available (see Key Resources Table). Assembly of the device requires soldering of two batteries (connected in series) with the LED and reed-switch in series. First, the LED is attached to an optical cannula using an epoxy resin adhesive with a refraction index similar to the optic fiber. For optimal alignment, the LED is connected to a power supply, fixed on a stereotactic holder, and positioned to yield the maximal light intensity as measured at the tip of the fiber. Upon optimal positioning, adhesive is applied, and the LED is pressed toward the optical cannula. Following soldering of the adhered LED to the rest of the components, the circuit is gently folded to form a compact structure and covered with dental cement and quinine to prevent potential damage by cage-mates. Prior to implantation, the fiber is cut according to the dorso-ventral coordinates of the brain region of interest, with an additional 1 mm to account for skull thickness and better fixation of the device on the skull (Video S1). To enable remote and unattended activation of the devices in our semi-natural arenas, software-controlled electromagnets were installed on the feeders enabling optogenetic stimulation of a given mouse during feeding (Figure 1C; Video S2). To better approximate physiological activation of neurons, we chose to use the Stabilized Step Function Opsin (SSFO), which upon activation by a single light pulse leads to prolonged (approximately 30 min) sub-threshold depolarization (Yizhar et al., 2011), sensitizing the cell to afferent inputs rather than inducing firing directly. The battery power of our device is sufficient for approximately 215 pulses of 2 s, at a light intensity of 2.8 ± 0.4 milliwatt×mm^{-2} at the tip of a single 5 mm long fiber of 0.4 mm diameter (Figure 1D). To confirm that our device produces sufficient light intensity for effective activation of considerable target volumes using SSFO, we mapped the spread of blue light (468 nm) in a 3 mm thick brain slice (Figure 1E). This provided an estimated 1.75 mm^3 of brain tissue being illuminated with light intensity above 8 microwatt×mm^{-2}, the lowest reported functional light intensity for SSFO (Yizhar et al., 2011).

Prolonged Wireless Optogenetic Activation of PVN-OT Neurons Triggers OT Release without Receptor Desensitization

Next, using our wireless optogenetic device, we aimed to establish a protocol for prolonged activation of the OTergic system in a way that would not induce desensitization of the OT receptors (OTRs), as is typically seen in continuous activation by OT or synthetic agonists leading to receptor internalization (Jurek and Neumann, 2018; Peters et al., 2014). We therefore targeted the OT neurons in the PVN, which are the source of most OT forebrain projections (Knobloch et al., 2012). To achieve specific targeting of PVN-OT neurons, we generated transgenic mice expressing Cre-recombinase specifically in OT neurons (*Oxt::Cre*; see STAR Methods). To transduce the SSFO into PVN-OT neurons, we used a Cre-dependent adeno-associated viral (AAV) vector that also expresses eYFP as a marker (DIO-SSFO-eYFP; Figures S1A and S1B). We delivered the viral vector in a single stereotaxic injection just above the dorsal part of the PVN such that it spread through the entire PVN. Following

Please cite this article in press as: Anpilov et al., Wireless Optogenetic Stimulation of Oxytocin Neurons in a Semi-natural Setup Dynamically Elevates Both Pro-social and Agonistic Behaviors, Neuron (2020), https://doi.org/10.1016/j.neuron.2020.05.028

CellPress
OPEN ACCESS

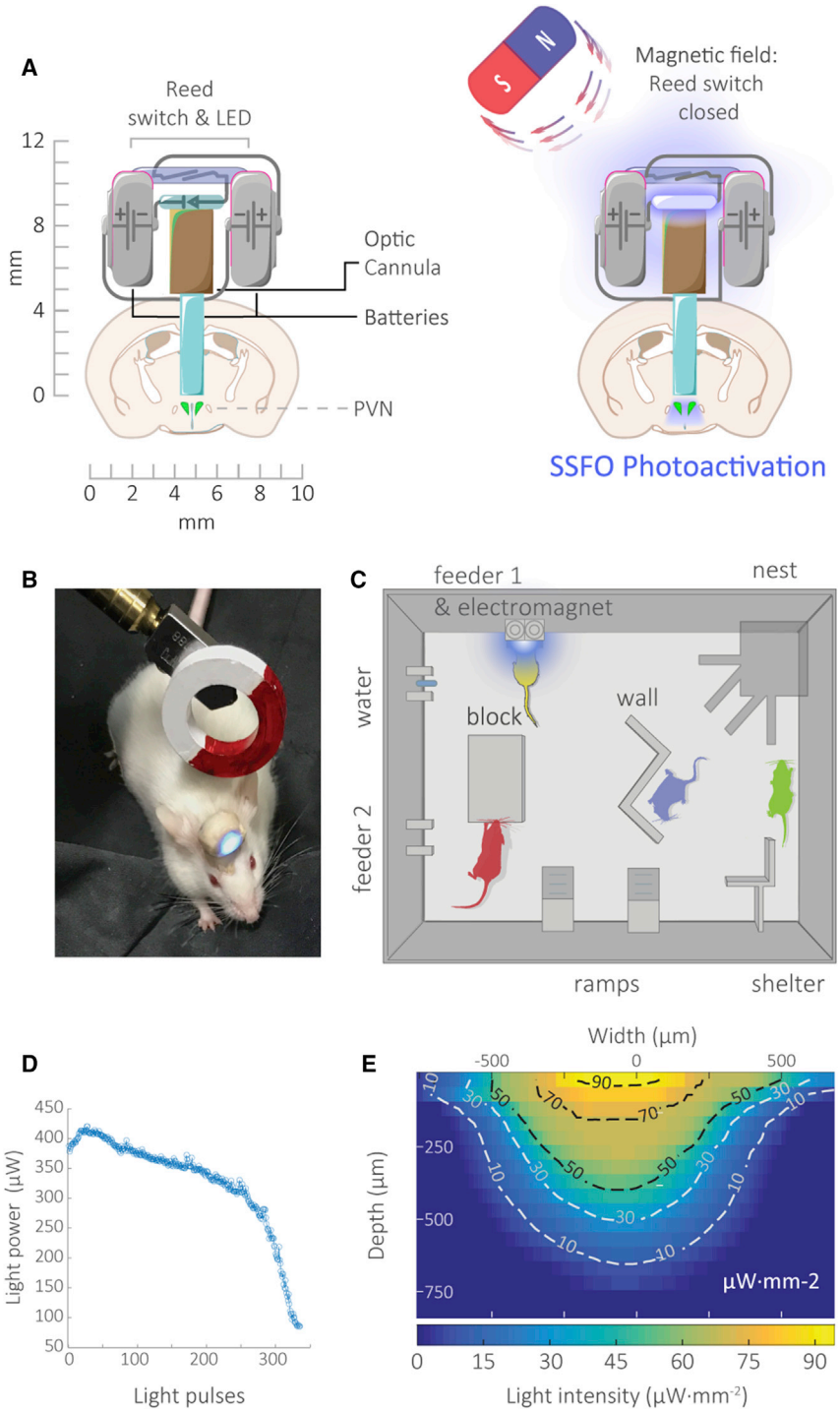

Figure 1. A Wireless Device for Prolonged Optogenetic Manipulation in a Semi-natural Setup

(A) Schematic illustration of the wireless device. Two batteries are connected in series to an LED through a magnetic-field dependent reed-switch. The LED is attached on top of an optic cannula positioned above the dorsal part of the PVN.

(B) A device mounted on a freely behaving mouse activated by a magnet.

(C) Schematic illustration of the semi-ethological arena and software-controlled electromagnet installed on the feeder. The arena consists of an open 70 × 50 cm box containing a nest, feeders, water, elevated areas, and barriers.

(D) Light power emitted at the tip of the optic fiber as a function of the number of 2 s light pulses. Battery capacity is sufficient for over 215 pulses.

(E) Section through a 3D map of blue light intensity along the axis of an illuminating fiber in gray matter. The slice was imaged from below as the fiber was lowered through. The section is superimposed with a contour map of iso-intensity lines corresponding to light intensity levels. Light intensity ≥ 8 microwatt×mm^{-2} is sufficient for effective SSFO photoactivation.

See also Videos S1 and S2.

injection, the wireless optogenetic device was implanted on the head with the single optic fiber lowered into the brain, so that the tip is positioned just above the dorsal part of the PVN.

The transgene penetrance and specificity were evaluated by crossing *Oxt::Cre* mice with Ai9 reporter mice (Madisen et al., 2010) and immunostaining for OT. In the 5 brains assessed, an average of 75.5% ± 12% of tdTomato$^+$ cells in the PVN co-expressed OT and 96% ± 4% of OT$^+$ cells co-expressed tdTomato (Figures 2A and 2B). SSFO expression and spread in the PVN in *Oxt::Cre*$^+$ mice using the single stereotaxic injection technique was as expected (Figure S1B).

To confirm that the typical functional characteristics of SSFO are preserved in our target population, we performed targeted whole-cell patch-clamp recordings in the PVN in acute brain slices from *Oxt::Cre*$^+$ mice injected with the SSFO viral vector (Figures 2C and 2D). In each recorded cell, the application of a 1 s blue light pulse (488 nm) induced membrane depolarization, accompanied in some cases by action potential firing. This depolarization slowly decayed with time (approximately 30 min) to the resting membrane potential (Figure 2C). The mean amplitude of SSFO-induced depolarization was 10.1 ± 0.66 mV. Deactivation of the SSFO with a 10 s green light pulse (561 nm) completely reversed this effect back to baseline levels (Figure 2D; 488 nm: 10.1 ± 0.66 mV versus 561 nm: −0.4 ± 0.49 mV, relative to pre-stimulation resting membrane potential; one-tailed exact paired permutation test, $p = 6.1 \times 10^{-5}$, n = 14 cells). Superimposition of the blue light intensity map with an atlas figure of coronal brain section (Franklin and Paxinos, 2008) suggested that the spread of light is sufficient to fully cover the PVN with light

Please cite this article in press as: Anpilov et al., Wireless Optogenetic Stimulation of Oxytocin Neurons in a Semi-natural Setup Dynamically Elevates Both Pro-social and Agonistic Behaviors, Neuron (2020), https://doi.org/10.1016/j.neuron.2020.05.028

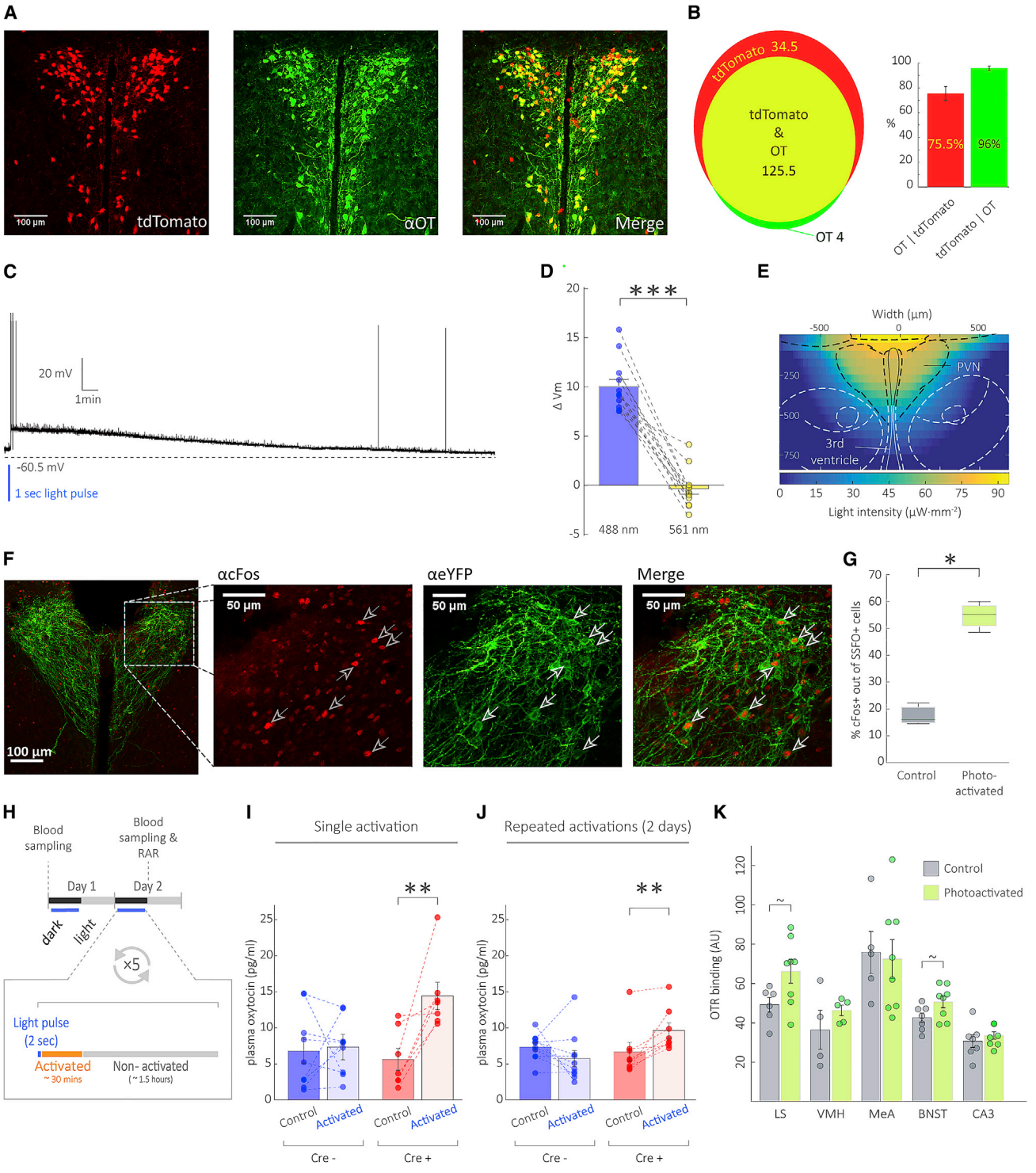

Figure 2. Prolonged Wireless Optogenetic Activation of PVN-OT Neurons Triggers OT Release without Receptor Desensitization

(A) Coronal brain sections at the level of the PVN showing the co-localization of Cre-dependent tdTomato reporter (red) with an anti-OT (αOT) antibody (green). Scale bars, 100 μm.

(B) Venn diagram describing the mean numbers of cells expressing tdTomato, OT or both (n = 5 mice). 96% of OT-expressing cells co-express tdTomato (right panel); data are means ± SEM.

(C) Representative current-clamp recording of SSFO activation in a PVN-OT neuron. A 1 s light pulse (488 nm) induces depolarization of the cell membrane followed by slow spontaneous decay of SSFO activity over a period of 30 min.

(legend continued on next page)

Please cite this article in press as: Anpilov et al., Wireless Optogenetic Stimulation of Oxytocin Neurons in a Semi-natural Setup Dynamically Elevates Both Pro-social and Agonistic Behaviors, Neuron (2020), https://doi.org/10.1016/j.neuron.2020.05.028

intensity levels necessary for effective activation of the SSFO ($I > 8$ microwatt$\times \cdot mm^{-2}$; Figure 2E). To demonstrate that the device can successfully activate PVN-OT neurons, we applied c-Fos immunostaining following a single 2 s light pulse in Cre^+ mice transduced with SSFO. The percentage of SSFO-infected cells that co-expressed c-Fos was significantly higher in the PVNs of photoactivated mice compared to non-activated controls (Figures 2F, 2G, and S1C; one-tailed Mann-Whitney test, $U = 0$, $p = 0.0286$, $n = 4$ and 3 mice for activated and control, respectively). To confirm that neuronal activation indeed leads to neuropeptide release, we measured plasma OT levels in Cre^+ and Cre^- mice injected with SSFO. For measurement of OT levels by radioimmunoassay (RIA), submandibular blood was collected under gentle anesthesia 3 min after a single light pulse, as well as following two consecutive days of repeated activations, every 2 h during the dark phase, between 10:00 and 18:00 (a total of five activations; Figure 2H). In both cases, SSFO-mediated photoactivation of PVN-OT neurons led to a significant increase in plasma OT in Cre^+ but not Cre^- mice (Figures 2I–2J; single activation: Cre^+, two-tailed paired permutation test, $p = 0.0156$, $n = 7$; Cre^-, two-tailed paired permutation test, $p = 0.7891$, $n = 9$. Repeated activation: Cre^+, two-tailed paired permutation test, $p = 0.00778$, $n = 8$; Cre^-, two-tailed paired permutation test, $p = 0.0209$, $n = 10$). This indicates that even a mild depolarization results in systemic OT release and, conversely, that the OT content of the neurons is not depleted following 2 days of activation. Importantly, we used receptor autoradiography (RAR) in several brain regions relevant to social behavior to confirm that our prolonged photoactivation protocol did not lead to OTR internalization: OTR binding in the medial amygdala (MeA), ventromedial hypothalamus (VMH), and hippocampal Cornu Ammonis 3 (CA3) did not differ significantly between photoactivated and control mice (Figures 2K and S1D–S1F; two-tailed permutation test, MeA: $p = 0.83$, $n = 5$ and 8 mice for activated and control, respectively; VMH: $p = 0.33$, $n = 5$ and 4 mice for activated and control, respectively; CA3: $p = 0.45$, $n = 8$ and 7 mice for activated and control, respectively). Intriguingly, there was a trend for increased OTR binding in the lateral septum (LS) and bed nucleus of the *stria terminalis* (BNST) following activation (Figures 2K, S1G, and S1H; two-tailed permutation test, LS: $p = 0.0506$, $n = 8$ and 6 mice for activated and control, respectively; BNST: $p = 0.065$, $n = 8$ and 7 mice for activated and control, respectively). Following these validations, we went on to use the same repeated photoactivation protocol in behavioral experiments.

Prolonged Wireless Optogenetic Release of OT Reduces Aggressive Behavior and Increases Self-Grooming in the RI Paradigm

Several studies have employed the RI paradigm to demonstrate a reduction in aggressive behaviors upon treatment with exogenous OT (Calcagnoli et al., 2013, 2014, 2015; Jong et al., 2014; Karpova et al., 2016) or an increase in such behaviors in animals genetically lacking OT or OTR (Dhakar et al., 2012; Pagani et al., 2015; Ragnauth et al., 2005; Takayanagi et al., 2005). These findings have led to the notion that OT generally reduces aggression. Importantly, the potential confounds of receptor desensitization during pharmacological treatment, and developmental effects in genetic KOs, can be eliminated with an optogenetic approach. Thus, we next sought to investigate our prolonged photoactivation regime in the RI paradigm.

Cre^+ and Cre^- male mice underwent stereotaxic virus injection and device implantation in a single surgical procedure at the age of 10 weeks and, following recovery, were housed in a large cage with a wild-type (WT) female for 6 days to increase territoriality. On day 7, after removing the female from the cage, we activated the wireless device using a magnet every 2 h during the dark phase, as described above. The next day we activated the devices at the beginning of the dark phase and then followed with an intraperitoneal (i.p.) injection of either the OTR antagonist L-368,899 (OTR-A; Cre^+ mice only; Cre^+|OTR-A) or saline (both Cre^+ and Cre^- mice; Cre^+|saline and Cre^-, respectively), 90 min later. The device was activated again 30 min following injection, immediately before the beginning of the behavioral test (Figure 3A). The total duration of aggressive behaviors (namely, attacks, offensive upright posture, and chasing; see STAR Methods, Method Details) was markedly reduced in Cre^+|saline mice compared to Cre^- mice (Figures 3B and S2C; Kruskal-Wallis test, chi-square test = 6.08, df = 2, $p = 0.0477$; Dunn-Sidak post hoc comparisons: Cre^+|saline versus Cre^- $p = 0.04952$, Cre^+|OTR-A versus Cre^- $p = 0.90788$). This difference was abolished by

(D) Quantification of the SSFO-induced membrane depolarization or inactivation (10 s green light pulse, 561 nm) in PVN-OT neurons. Data are means ± SEM; ***$p < 0.001$, permutation test.

(E) Superimposition of a blue light intensity map in a brain slice with a coronal atlas figure at the level of the PVN. PVN is fully included within an area illuminated with supra-optimal light intensity for SSFO activation (>8 microwatt$\times mm^{-2}$).

(F) Representative image of cFos (red) and eYFP (green) immunostaining. Arrows show co-expression of cFos in photoactivated $SSFO^+$ neurons. Scale bars, 100 (main image) and 50 μm (inset).

(G) A significantly higher percent of $SSFO^+$ cells co-expressed cFos following photoactivation compared to non-activated subjects; median ± 1.5 interquartile range; *$p < 0.05$, Mann-Whitney test.

(H) Photo-activation timeline: Devices were activated approximately every 2 h during the dark phase of 2 consecutive days. Blood was sampled 3 min following a single activation and following 2 days of repeated activations.

(I) Plasma OT levels significantly increased in Cre^+ mice following single activation.

(J) Plasma OT levels significantly increased in Cre^+ mice following 2 days of repeated activations. No significant differences were observed in Cre^- mice; data are means ± SEM.

(K) Receptor autoradiography (RAR) indicates that our prolonged activation regime did not lead to reduction of OTR binding in the lateral septum (LS), ventromedial hypothalamus (VMH), medial amygdala (MeA), bed nucleus of the *stria terminalis* (BNST), or hippocampal Cornu Ammonis 3 (CA3); For (I–K): data are means ± SEM; **$p < 0.01$, permutation test.

See also Figure S1.

Please cite this article in press as: Anpilov et al., Wireless Optogenetic Stimulation of Oxytocin Neurons in a Semi-natural Setup Dynamically Elevates Both Pro-Social and Agonistic Behaviors, Neuron (2020), https://doi.org/10.1016/j.neuron.2020.05.028

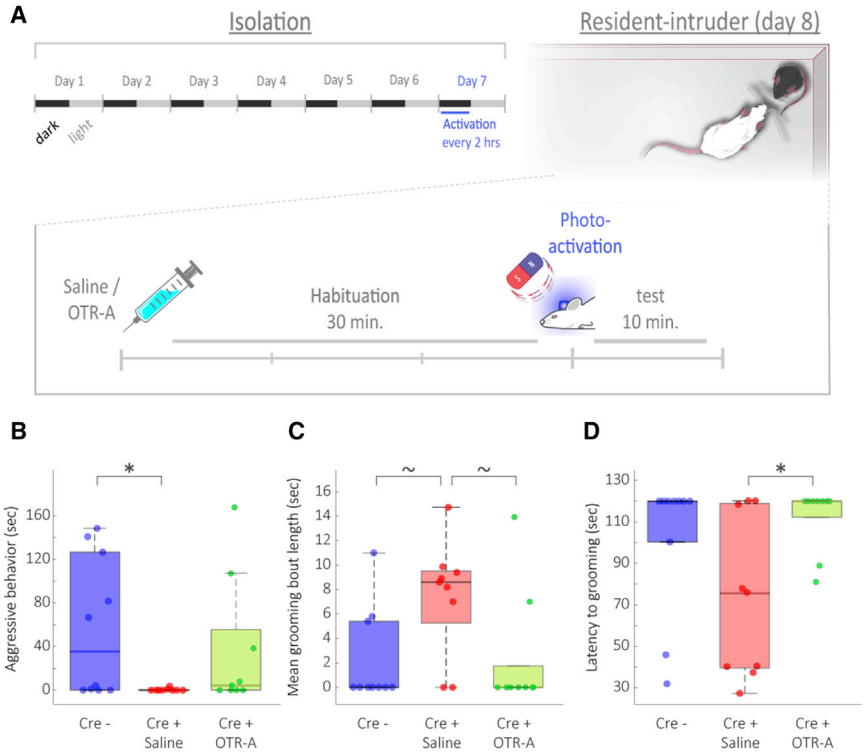

Figure 3. Prolonged Wireless Optogenetic Release of OT Reduces Aggressive Behavior and Increases Self-Grooming in Resident-Intruder Paradigm

(A) Experimental timeline. Prior to testing, mice were housed in a large cage with a WT female for 6 days. On the 7th day, the female was removed at the beginning of the dark phase, and the devices were the activated every 2 h. At the beginning of the dark phase of day 8, mice were injected with either saline or OTR-A 30 min before photoactivation and the introduction of the intruder mouse.

(B) Aggressive behavior was significantly reduced in saline-treated, but not OTR-A-treated, Cre^+ mice compared to Cre^- controls.

(C) Mean length of grooming bouts in Cre^+|saline mice was longer than in other treatments to an extent approaching statistical significance.

(D) Cre^+|saline mice displayed significantly shorter latency to first grooming bout compared to Cre^+|OTR-A mice. All data represent medians ±1.5 interquartile range; *$p < 0.05$, Kruskal-Wallis with post-hoc.

See also Figure S2, Table S1, and Video S3.

administration of OTR-A, suggesting an OTR-mediated reduction in aggression caused by our manipulation. To rule out the possibility that the reduction in aggressive behaviors was due to an increase in other behaviors in the Cre^+|saline group, we quantified locomotion and found no significant differences in either the total distance covered by the mice or the percentage of distance covered while engaging in social/non-social behavior (Figure S2A; Kruskal-Wallis test, total distance covered: chi-square test = 1.34, df = 2, p = 0.51; percentage of distance while engaging in social behavior: chi-square test = 3.12, df = 2, p = 0.21). Furthermore, no difference was found in the percentage of time spent exhibiting social/non-social behavior (Figures S2B and S2C; Kruskal-Wallis test, chi-square test = 1.6, df = 2, p = 0.45; see also Table S1). As additional support for central OT release, we investigated self-grooming behavior, which has been previously shown to be induced by central OTR activation (Amico et al., 2004; Marroni et al., 2007; Pedersen et al., 1988) and more recently by chemogenetic activation of OT neurons (Grund et al., 2019). The mean duration of grooming bouts was highest in Cre^+ mice treated with saline (Figure 3C). Kruskal-Wallis analysis revealed a significant effect of treatment on this measure (chi-square test = 7, df = 2, p = 0.0302); post hoc Dunn's test found that the differences between the Cre^+|saline group and the two other groups approached significance (Cre^+|saline versus Cre^- p = 0.06315; Cre^+|saline versus Cre^+|OTR-A p = 0.06254). Furthermore, latency to the first grooming bout was significantly shorter in the Cre^+|saline group compared to Cre^+|OTR-A group (Figure 3D; Kruskal-Wallis test, chi-square test = 7.57, df = 2, p = 0.0228; Dunn-Sidak post hoc comparison: Cre^+|saline versus Cre^+|OTR-A p = 0.02864). Thus, repeated wireless photoactivation of PVN-OT neurons induced the expected behavioral consequences of OT signaling in the RI paradigm.

Prolonged Wireless Optogenetic Activation of PVN-OT Neurons Dynamically Elevates Both Pro-Social and Agonistic Behaviors in Groups of Male Mice

According to the social salience hypothesis of OT, its effect might depend on social context. Thus, we asked how repeated activation of PVN-OT neurons would affect behavior over time in group-housed mice in an enriched environment. To this end, we assembled homogeneous Cre^+ or Cre^- groups of 4 male littermates at weaning age (3 weeks). Mice underwent surgery at the age of 10 weeks, recovered in the original group home cages, and were introduced into the social arenas 3 weeks later. Following 4 days of habituation, the devices were activated as mice entered the feeder for 2 additional days, approximately every 2 h during the dark phase for at least 2 s (Figure 4A). During the entire experiment, feeders were accessible during randomly chosen time periods, for a total of 5 h during the dark phase (see STAR Methods, Method Details), in order to increase competition between group members. During the light phase, feeders remained closed. Photoactivation events were visually monitored to make sure that each mouse was activated in the appropriate time window.

First, we were interested in whether OT-induced self-grooming, as observed in the RI paradigm, is reproduced in the group context. Grooming behavior was scored by observers blind to the genotype of the mice in the first 5 min after each photoactivation, on both activation days. Photoactivation significantly increased the length of self-grooming bouts, and shortened the

Please cite this article in press as: Anpilov et al., Wireless Optogenetic Stimulation of Oxytocin Neurons in a Semi-natural Setup Dynamically Elevates Both Pro-social and Agonistic Behaviors, Neuron (2020), https://doi.org/10.1016/j.neuron.2020.05.028

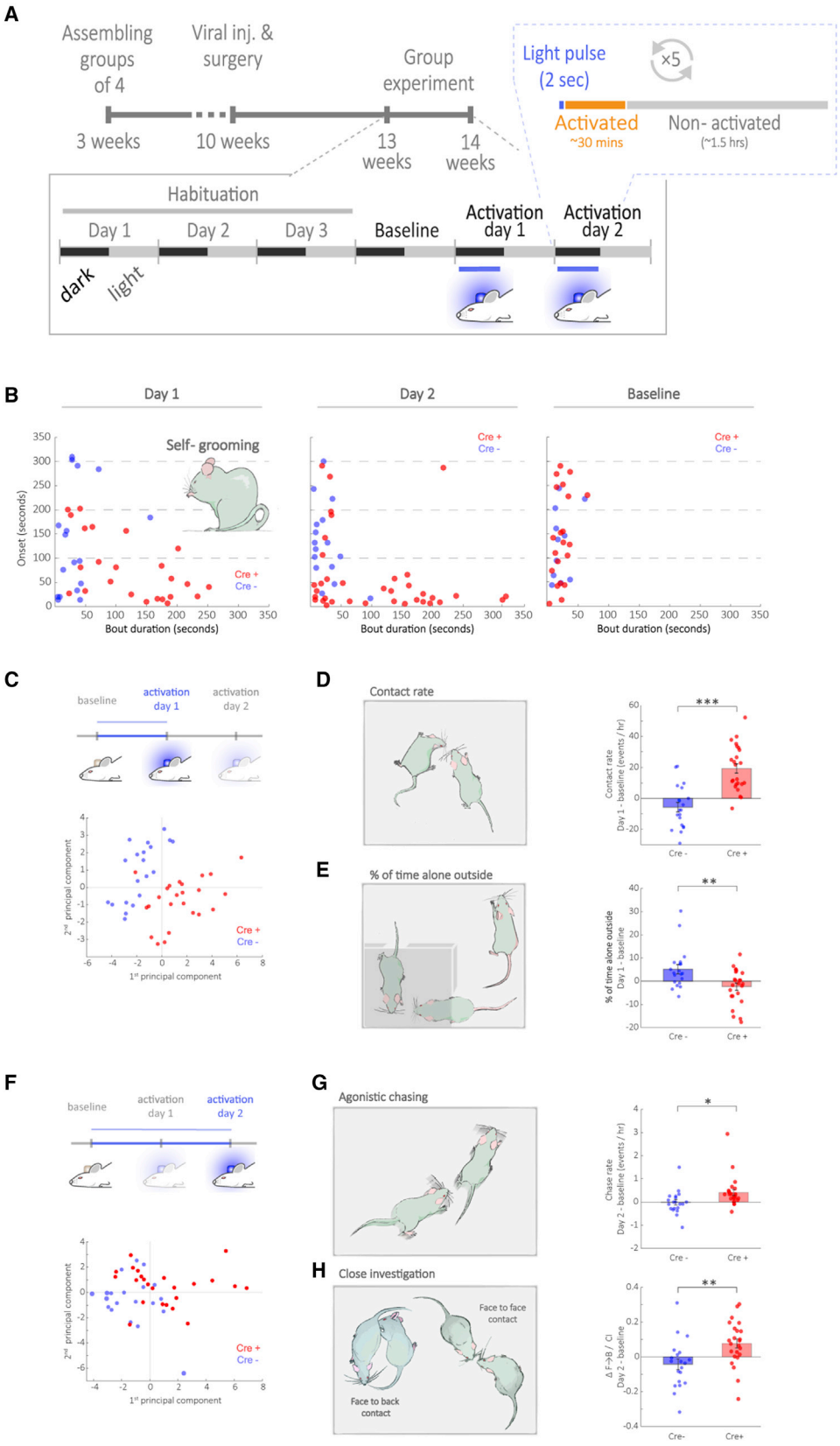

(legend on next page)

Please cite this article in press as: Anpilov et al., Wireless Optogenetic Stimulation of Oxytocin Neurons in a Semi-natural Setup Dynamically Elevates Both Pro-social and Agonistic Behaviors, Neuron (2020), https://doi.org/10.1016/j.neuron.2020.05.028

latency to the first bout, in Cre^+ but not Cre^- mice on both activation days (Figure 4B, S3A, and S3B; Video S3; paired one-tailed permutations test; bout length: Cre^-, $p_{day1} = 0.188$, $p_{day2} = 0.125$; Cre^+, $p_{day1} = 0.031$, $p_{day2} = 0.016$; latency: Cre^-, $p_{day1} = 0.41$, $p_{day2} = 0.34$; Cre^+, $p_{day1} = 0.031$, $p_{day2} = 0.016$), as well as increasing the probability of a grooming bout during the observed time window (Figure S3C, paired one-tailed permutations test: Cre^-, $p_{day1} = 0.5$, $p_{day2} = 0.22$; Cre^+, $p_{day1} = 0.031$, $p_{day2} = 0.016$).

We analyzed 21 readouts from our automated tracking system, related to individual and dyadic behaviors, that are calculated based on the locations of individual mice in the arena (Forkosh et al., 2019; Shemesh et al., 2013, 2016). To examine the effects of PVN-OT activation, we focused on the behavioral change from baseline (measured on day 4) to the value on either day of activation. First, we quantified the degree of separation between Cre^+ and Cre^- groups over all 21 behaviors, which on both activation days was more extreme than expected by chance (Figures S3D and S3E; multivariate permutation test on 1×10^5 permutations; activation day 1 $p < 1 \times 10^{-5}$, activation day 2 $p = 0.00047$). Next, for visual inspection of this behavioral response in a 2-dimensional plot, we performed principal component analysis (PCA). The first 2 principal components (PC1 and PC2) cumulatively explained 41% (activation day 1 versus baseline) and 44% (activation day 2 versus baseline) of the total variance in the data, which was in both cases significantly higher than expected by chance, as calculated by randomly permuting the data (see STAR Methods, Quantification and Statistical Analysis; Figures S3F and S3G; two-tailed permutation test on 1×10^7 permutations, PC1 $p = 4.2 \times 10^{-7}$, PC2 $p = 0.00088$). Although the PCA was done blindly to the genotype of the subjects, Cre^+ and Cre^- were almost perfectly linearly separated in this 2-PC space (Figures 4C and 4F). To examine which behavioral readouts contribute to this separation, we inspected the correlations between behavioral readouts and the scores on the first two PCs: on the first activation day, PC1 scores were positively correlated with affiliative behaviors, such as rates of approach and contact between conspecifics, and negatively correlated with time spent alone outside the nest, a prototypical asocial behavior (Figure S3H). To quantify the difference between treatment groups specifically in these behavioral readouts, we compared the change in these behaviors from baseline (day 4) to activation day 1 between Cre^+ and Cre^- mice. Cre^+ mice had a significantly higher increase in contact rate (Figure 4D; two-tailed permutation test, $p = 9 \times 10^{-7}$). Similarly, time spent alone outside the nest decreased in Cre^+ mice but increased in Cre^- from baseline to activation day 1 (Figure 4E; two-tailed permutation test, $p = 0.0028$).

On the second day of activation, the correlations between specific behaviors and PC1 scores remained largely similar to the previous day, and, accordingly, the change from baseline in contact rate and time alone outside the nest remained larger in Cre^+ mice (Figures S3J and S3K; two-tailed permutation tests, contact rate $p = 0.00098$, time alone $p = 0.02037$). In contrast, PC2 on this day was positively correlated with readouts related to velocity and chase-escape behavior (Figure S3I). Thus, we compared the change in agonistic chase behavior from baseline to activation day 2 between the groups, measured as rates of chases per hour (Video S4). The increase in this behavior was significantly larger in Cre^+ mice compared to Cre^- mice (Figure 4G; two-tailed permutation test, $p = 0.0132$). Importantly, this difference was absent on the first day of activation (Figure S3L; two-tailed permutation test, $p = 0.8218$). Next, to confirm a general increase in agonistic behavior, we sought an additional measure for this behavioral domain. Observations of mice colonies in a visible burrow system have shown that approach toward the back of a conspecific more often induces flight than approach to the front and thus may reflect an offensive motivation (Arakawa et al., 2007). Additionally, anogenital sniffing and attack behavior have been shown to be regulated by a common neuronal population (Lee et al., 2014). Thus, we compared the proportion of face-to-face (F→F) versus face-to-back (F→B) approaches in randomly sampled contact events from Cre^+ and Cre^- groups. Cre^+ mice had a significantly larger increase from baseline in the proportion of F→B approaches on the second activation day (Figure 4H, two-tailed permutation test, $p = 0.0047$). Importantly, there was no difference in F→B approaches on the first day of activation (Figure S3M, two-tailed permutation test, $p = 0.4643$). When we examined the dynamics of approach and chasing behaviors in a 1 h window preceding and following photoactivation, we found that the changes in these behaviors were not time-locked to photoactivation on either day (Figures S4A and S4B; ANOVA on linear mixed effects model with post hoc Tukey comparison; Approaches day 1:

Figure 4. Prolonged Wireless Optogenetic Activation of PVN-OT Neurons in a Group of Littermates Dynamically Elevates Both Pro-Social and Agonistic Behaviors

(A) Scheme of experimental timeline. Mice were grouped at weaning into groups of 4 males of the same genotype (Cre^+ versus Cre^-). At age 10 weeks, mice underwent surgery for viral injection and device implantation. Following 3 weeks of recovery, groups were introduced into the arenas for 4 days of undisturbed baseline recording, followed by 2 days of photoactivation every 2 hr during the dark phase.

(B) Scatterplots depicting the onset of self-grooming after photoactivation against bout duration. Days 1 and 2: self-grooming bouts in Cre^+ mice were significantly longer compared to Cre^- and occurred with a shorter onset following activation. Baseline: no difference between Cre^+ and Cre^- mice was observed in bout length or onset.

(C) Principal component analysis (PCA) was done on differential values of activation day 1 from baseline. Below: scatterplot of the scores on the first two principal components (PCs).

(D) Increase in contact rate in Cre^+ was significantly larger than in Cre^- mice from baseline to activation day 1.

(E) Decrease in time spent alone outside the nest by Cre^+ was significantly greater than in Cre^- mice from baseline to activation day 1.

(F) PCA was done on differential values of activation day 2 from baseline. Below: scatterplot of the scores on the first two PCs.

(G) Increase in aggressive chase rate was significantly larger in Cre^+ than in Cre^- mice from baseline to activation day 2.

(H) Social encounters with the nose directed toward the face or the back/tail region of a conspecific in close vicinity (<3.5 cm) were automatically and randomly sampled and defined as close investigation (CI). The change in the proportion of face-to-back (F◇B) contacts out of randomly sampled CI events after 2 days of repeated photoactivation was significantly larger in Cre^+ compared to Cre^- mice.

All data represent means ± SEM; *p < 0.05, **p < 0.01, ***p < 0.001, permutation test. See also Figures S3 and S4 and Video S4.

Genotype – $F_{1/8.07}$ = 6.8, p = 0.031, Time – $F_{39/1167.03}$ = 4.22, p = 5.347e^{-16}, Genotype*Time – $F_{39/1167.03}$ = 2.32, p = 1.036e^{-5}; Approaches day 2: Genotype – $F_{1/68.37}$ = 14.24, p = 0.00034, Time – $F_{39/1402.07}$ = 1.523, p = 0.0212, Genotype*Time – $F_{39/1402.07}$ = 1.43, p = 0.043; chases day 1: Genotype – $F_{1/8.58}$ = 0.0485, p = 0.83, Time – $F_{39/1167.03}$ = 0.822, p = 0.77, Genotype*Time – $F_{39/1167.03}$ = 0.877, p = 0.68; chases day 2: Genotype – $F_{1/116.87}$ = 0.57, p = 0.45, Time – $F_{39/1404.49}$ = 0.54, p = 0.99, Genotype*Time – $F_{39/1404.49}$ = 0.846, p = 0.74). Importantly, approach and chase behavior, as well as time alone outside the nest, were independent of dominance rank (Figures S4C–S4G; Pearson correlation). We also tested whether individual stable traits extracted from 60 behaviors measured in our social boxes ("identity domains" - IDs, Forkosh et al., 2019) were altered following prolonged activation of PVN-OT neurons. As expected, when comparing the changes in the 4 meaningful IDs on either day of activation versus baseline, we found no significant differences between Cre^{+} and Cre^{-} mice (Figures S4H–S4K; ANOVA on linear mixed effects model; ID1: Genotype – $F_{1/42}$ = 1.2918, p = 0.2622, Day – $F_{1/42}$ = 0.0033, p = 0.9541, Genotype*Day – $F_{1/42}$ = 0.4157, p = 0.5226; ID2: Genotype – $F_{1/9}$ = 0.3787, p = 0.5535, Day – $F_{1/42}$ = 0.0004, p = 0.9848, Genotype*Day – $F_{1/42}$ = 0.0158, p = 0.9007; ID3: Genotype – $F_{1/9}$ = 0.0319, p = 0.8623, Day – $F_{1/42}$ = 0.0044, p = 0.9475, Genotype*Day – $F_{1/42}$ = 0.6173, p = 0.4365; ID4: Genotype – $F_{1/9}$ = 0.2903, p = 0.6031, Day – $F_{1/42}$ = 0.0020, p = 0.9646, Genotype*Day – $F_{1/42}$ = 0.4223, p = 0.5193).

Taken together, these results suggest that in the context of a group of familiar males, prolonged PVN-OT neuronal activation leads to a dynamic behavioral shift, comprising an immediate elevation in social interest, which can be interpreted as pro-social behavior, along with a delayed increase in agonistic behavior.

DISCUSSION

Advanced molecular and genetic tools for neuronal manipulation in animal models hold great promise for the quest of deciphering the mechanisms underlying psychiatric disorders. However, in order to fully utilize these tools, behavioral paradigms must advance as well. Though the widely used reductionist tests have the advantage of better controllability, they still raise questions regarding translatability—if a behavioral task is far enough removed from an animal's natural environment or behavioral repertoire, it may reflect neural or behavioral responses that are not used naturally (Krakauer et al., 2017). Thus, holistic approaches for measuring behavior should complement the current well-established methodologies. Unfortunately, understanding of the ethology of mice and rats in the wild is still lacking, and this gap in knowledge and methodology has been acknowledged as a major challenge in the field (Anderson and Perona, 2014; Blanchard et al., 2013; Kondrakiewicz et al., 2019). Here, we present an approach that combines the known advantages of optogenetics—namely, highly specific and precise manipulation of neuronal activity—with the growing need for ethologically relevant behavioral readouts, by introducing wireless optogenetic devices into a semi-natural group environment.

While several technologies for wireless light delivery into brain tissue have already been published (Dagnew et al., 2017; Emara et al., 2018; Kim et al., 2013; McCall et al., 2013; Montgomery et al., 2015; Qazi et al., 2018, 2019; Shin et al., 2017; Wentz et al., 2011), this is, to our knowledge, the first study demonstrating the use of such technology in a semi-natural environment and over multiple days, using an affordable and easy-to-assemble device.

We used our approach to investigate the social salience hypothesis of OT (Shamay-Tsoory and Abu-Akel, 2016). While seminal studies in male-male and male-female rodent pairs have contributed to the notion of OT as a facilitator of affiliative behaviors (Lukas et al., 2011; Williams et al., 1994; Witt et al., 1992), recent findings also provide evidence of antisocial effects of OT (van Anders et al., 2013; Bartz et al., 2011; Beery, 2015). The social salience hypothesis explains these apparently contradictory effects by suggesting that OT acts to regulate the salience of social cues, depending on contextual and individual variation. Our methodology, which combines a holistic semi-natural phenotyping approach with advanced neuronal manipulation, in parallel with controlled classic tests, is ideal to address such behaviorally complex questions. We first demonstrate that repeated activation of PVN-OT neurons on the day before and the morning of the RI test leads to a reduction in agonistic behavior, in accordance with studies using OT genetic models and acute pharmacological manipulations. However, in a semi-natural group environment, the social dynamics are more complex: we initially observe a clear increase in social interest between mice (more approaches and contacts), which can be interpreted as an increase in pro-social behavior. On the second day of manipulation, however, this trend is accompanied by an increase in agonistic behaviors such as anogenital sniffing and aggressive chases. While most classic behavioral paradigms are set up to dictate a pre-defined and specific social context, a group setting imposes a dynamic set of social stimuli. Thus, in our hands, the group environment with limited food availability profoundly affects the behavioral outcome of activating PVN-OT neurons, leading to a different result than the classic RI test. This finding is in agreement with the social salience hypothesis and emphasizes the importance of observing behavioral changes over longer time periods, rather than only following acute manipulation, and in a variety of contexts. In this vein, it would be important to also investigate the effect of a similar manipulation in female mice, as well as males.

While the majority of studies investigating the role of OT in aggressive/agonistic behaviors have reported a mitigating effect (Arakawa et al., 2015; Calcagnoli et al., 2013, 2014, 2015; Dhakar et al., 2012; Jong et al., 2014; Karpova et al., 2016; Ragnauth et al., 2005; Sala et al., 2011; Takayanagi et al., 2005; Tan et al., 2019; Winslow et al., 2000; Zoratto et al., 2018), a few others have indicated that OT can potentially increase such behaviors (DeVries et al., 1997; Lazzari et al., 2013; Pagani et al., 2015). One study even showed the differential effects of OT in rats selectively bred for aggression or tameness toward humans, with a 5-day intranasal treatment reducing aggressive behavior in the aggressive strain but increasing it in the tame strain (Gulevich et al., 2019). Since OT is being explored as a therapeutic agent in human disorders affecting social behavior and cognition, such as social anxiety and ASD (Alvares et al., 2017; Guastella et al., 2009; Ooi et al., 2017), these findings are crucial to consider.

In conclusion, we believe that the combination of high-precision optogenetic manipulations with ethologically relevant

behaviors in a semi-natural environment is an important step toward more translatable, informative, and comprehensive neurobehavioral research in rodents.

STAR★METHODS

Detailed methods are provided in the online version of this paper and include the following:

- KEY RESOURCES TABLE
- RESOURCE AVAILABILITY
  - Lead Contact
  - Materials Availability
  - Data and Code Availability
- EXPERIMENTAL MODEL AND SUBJECT DETAILS
  - Generation of Oxt::Cre (Ires-Cre-Oxt::Ires-Flp-Avp) mice
  - Animals
- METHOD DETAILS
  - Fabrication of wireless optogenetic device
  - Specific SSFO expression in PVN-OT neurons
  - Stereotaxic injections and mounting of the wireless optogenetic device
  - Fur marking for video tracking
  - Light penetration in brain tissue
  - Electrophysiology
  - Immunohistochemistry and microscopy
  - OT levels in plasma
  - Receptor Autoradiography
  - Social arenas
  - Resident-intruder
- QUANTIFICATION AND STATISTICAL ANALYSIS

SUPPLEMENTAL INFORMATION

Supplemental Information can be found online at https://doi.org/10.1016/j.neuron.2020.05.028.

ACKNOWLEDGMENTS

The authors wish to thank Franck Touboul for assistance with DeepLabCut tracking, Dr. Jessica Keverne for writing and editing support and advice, and Dr. Ron Rotkopf for assistance with statistical analyses. A.C. is the incumbent of the Vera and John Schwartz Family Professorial Chair in Neurobiology at the Weizmann Institute and the head of the Max Planck Society–Weizmann Institute of Science Laboratory for Experimental Neuropsychiatry and Behavioral Neurogenetics gratefully funded by the Max Planck Foundation. This work is supported by an FP7 Grant from the European Research Council (260463, A.C.); a research grant from the Israel Science Foundation (1565/15, A.C.); and the ERANET Program, supported by the Chief Scientist Office of the Israeli Ministry of Health (3-11389, A.C.); the project was funded by the Federal Ministry of Education and Research under the funding code 01KU1501A (A.C.); I-CORE Program of the Planning and Budgeting Committee and The Israel Science Foundation (grant no. 1916/12 to A.C.); Ruhman Family Laboratory for Research in the Neurobiology of Stress (A.C.); research support from Bruno and Simone Licht; the Perlman Family Foundation, founded by Louis L. and Anita M. Perlman (A.C.); the Adelis Foundation (A.C.); and Sonia T. Marschak (A.C.).

AUTHOR CONTRIBUTIONS

Conceptualization, S.A., Y.S., and A.C.; Methodology, S.A., Y.S., O.F., H.H.-N., and A.D.; Software, A.B. and O.F.; Investigation, S.A., Y.S., N.E., JD, R.-E.H., V.E.M.O., and G.C.; Validation, S.A., Y.S., N.E., and H.H.-N.; Formal Analysis, S.A., Y.S., N.E., A.B., and J.D., V.E.M.O., S.K., N.F., and R.B.; Writing, N.E., S.A., and Y.S.; Visualization, S.A.; Funding Acquisition, A.C.; Resources, O.Y. and S.W.; Supervision: A.C., O.Y., S.W., and I.D.N.

DECLARATION OF INTERESTS

The authors declare no competing interests.

Received: February 7, 2020
Revised: May 6, 2020
Accepted: May 20, 2020
Published: June 15, 2020

REFERENCES

Alvares, G.A., Quintana, D.S., and Whitehouse, A.J.O. (2017). Beyond the hype and hope: Critical considerations for intranasal oxytocin research in autism spectrum disorder. Autism Res. *10*, 25–41.

Amico, J.A., Vollmer, R.R., Karam, J.R., Lee, P.R., Li, X., Koenig, J.I., and McCarthy, M.M. (2004). Centrally administered oxytocin elicits exaggerated grooming in oxytocin null mice. Pharmacol. Biochem. Behav. *78*, 333–339.

Anderson, D.J., and Perona, P. (2014). Toward a science of computational ethology. Neuron *84*, 18–31.

Arakawa, H., Blanchard, D.C., and Blanchard, R.J. (2007). Colony formation of C57BL/6J mice in visible burrow system: identification of eusocial behaviors in a background strain for genetic animal models of autism. Behav. Brain Res. *176*, 27–39.

Arakawa, H., Blanchard, D.C., and Blanchard, R.J. (2015). Central oxytocin regulates social familiarity and scent marking behavior that involves amicable odor signals between male mice. Physiol. Behav. *146*, 36–46.

Bartz, J.A., Zaki, J., Bolger, N., and Ochsner, K.N. (2011). Social effects of oxytocin in humans: context and person matter. Trends Cogn. Sci. *15*, 301–309.

Bates, D., Mächler, M., Bolker, B., and Walker, S. (2015). Fitting Linear Mixed-Effects Models Using lme4. J. Stat. Softw. *67*, 1.

Beery, A.K. (2015). Antisocial oxytocin: Complex effects on social behavior. Curr. Opin. Behav. Sci. *6*, 174–182.

Blanchard, D.C., Summers, C.H., and Blanchard, R.J. (2013). The role of behavior in translational models for psychopathology: functionality and dysfunctional behaviors. Neurosci. Biobehav. Rev. *37*, 1567–1577.

Calcagnoli, F., de Boer, S.F., Althaus, M., den Boer, J.A., and Koolhaas, J.M. (2013). Antiaggressive activity of central oxytocin in male rats. Psychopharmacology (Berl.) *229*, 639–651.

Calcagnoli, F., Meyer, N., de Boer, S.F., Althaus, M., and Koolhaas, J.M. (2014). Chronic enhancement of brain oxytocin levels causes enduring anti-aggressive and pro-social explorative behavioral effects in male rats. Horm. Behav. *65*, 427–433.

Calcagnoli, F., Kreutzmann, J.C., de Boer, S.F., Althaus, M., and Koolhaas, J.M. (2015). Acute and repeated intranasal oxytocin administration exerts anti-aggressive and pro-affiliative effects in male rats. Psychoneuroendocrinology *51*, 112–121.

Dagnew, R., Lin, Y.-Y., Agatep, J., Cheng, M., Jann, A., Quach, V., Monroe, M., Singh, G., Minasyan, A., Hakimian, J., et al. (2017). CerebraLux: a low-cost, open-source, wireless probe for optogenetic stimulation. Neurophotonics *4*, 045001.

De Dreu, C.K.W., Greer, L.L., Handgraaf, M.J.J., Shalvi, S., Van Kleef, G.A., Baas, M., Ten Velden, F.S., Van Dijk, E., and Feith, S.W.W. (2010). The neuropeptide oxytocin regulates parochial altruism in intergroup conflict among humans. Science *328*, 1408–1411.

De Dreu, C.K.W., Greer, L.L., Van Kleef, G.A., Shalvi, S., and Handgraaf, M.J.J. (2011). Oxytocin promotes human ethnocentrism. Proc. Natl. Acad. Sci. USA *108*, 1262–1266.

DeVries, A.C., Young, W.S., 3rd, and Nelson, R.J. (1997). Reduced aggressive behaviour in mice with targeted disruption of the oxytocin gene. J. Neuroendocrinol. *9*, 363–368.

Dhakar, M.B., Rich, M.E., Reno, E.L., Lee, H.J., and Caldwell, H.K. (2012). Heightened aggressive behavior in mice with lifelong versus postweaning knockout of the oxytocin receptor. Horm. Behav. *62*, 86–92.

Dine, J., Genewsky, A., Hladky, F., Wotjak, C.T., Deussing, J.M., Zieglgänsberger, W., Chen, A., and Eder, M. (2016). Local optogenetic induction of fast (20–40 Hz) pyramidal-interneuron network Oscillations in the in vitro and in vivo CA1 hippocampus: Modulation by CRF and enforcement of perirhinal theta activity. Front. Cell. Neurosci. *10*, 1–11.

Duque-Wilckens, N., Steinman, M.Q., Busnelli, M., Chini, B., Yokoyama, S., Pham, M., Laredo, S.A., Hao, R., Perkeybile, A.M., Minie, V.A., et al. (2018). Oxytocin Receptors in the Anteromedial Bed Nucleus of the Stria Terminalis Promote Stress-Induced Social Avoidance in Female California Mice. Biol. Psychiatry *83*, 203–213.

Eckstein, M., Scheele, D., Weber, K., Stoffel-Wagner, B., Maier, W., and Hurlemann, R. (2014). Oxytocin facilitates the sensation of social stress. Hum. Brain Mapp. *35*, 4741–4750.

Emara, M.S., Pisanello, M., Sileo, L., De Vittorio, M., and Pisanello, F. (2018). A Wireless Head-mountable Device with Tapered Optical Fiber-coupled Laser Diode for Light Delivery in Deep Brain Regions. IEEE Trans. Biomed. Eng. *66*, 1996–2009.

Ferretti, V., Maltese, F., Contarini, G., Nigro, M., Bonavia, A., Huang, H., Gigliucci, V., Morelli, G., Scheggia, D., Managò, F., et al. (2019). Oxytocin Signaling in the Central Amygdala Modulates Emotion Discrimination in Mice. Curr. Biol. *29*, 1938–1953.

Forkosh, O., Karamihalev, S., Roeh, S., Alon, U., Anpilov, S., Touma, C., Nussbaumer, M., Flachskamm, C., Kaplick, P.M., Shemesh, Y., and Chen, A. (2019). Identity domains capture individual differences from across the behavioral repertoire. Nat. Neurosci. *22*, 2023–2028.

Franklin, K., and Paxinos, G. (2008). The Mouse Brain in Stereotaxic Coordinates. The Coronal Plates and Diagrams (Academic Press).

Gagnon-Turcotte, G., Keramidis, I., Ethier, C., De Koninck, Y., and Gosselin, B. (2019). A Wireless Electro-Optic Headstage with a 0.13-μm Wireless Electro-Optic Headstage with a 0.13- Coronal Plates and Diagramsrepert. IEEE Trans. Biomed. Circuits Syst. *13*, 1036–1051.

Grund, T., Tang, Y., Benusiglio, D., Althammer, F., Probst, S., Oppenländer, L., Neumann, I.D., and Grinevich, V. (2019). Chemogenetic activation of oxytocin neurons: Temporal dynamics, hormonal release, and behavioral consequences. Psychoneuroendocrinology *106*, 77–84.

Guastella, A.J., Howard, A.L., Dadds, M.R., Mitchell, P., and Carson, D.S. (2009). A randomized controlled trial of intranasal oxytocin as an adjunct to exposure therapy for social anxiety disorder. Psychoneuroendocrinology *34*, 917–923.

Gulevich, R., Kozhemyakina, R., Shikhevich, S., Konoshenko, M., and Herbeck, Y. (2019). Aggressive behavior and stress response after oxytocin administration in male Norway rats selected for different attitudes to humans. Physiol. Behav. *199*, 210–218.

Guzmán, Y.F., Tronson, N.C., Jovasevic, V., Sato, K., Guedea, A.L., Mizukami, H., Nishimori, K., and Radulovic, J. (2013). Fear-enhancing effects of septal oxytocin receptors. Nat. Neurosci. *16*, 1185–1187.

Ho, J.S., Yeh, A.J., Neofytou, E., Kim, S., Tanabe, Y., Patlolla, B., Beygui, R.E., and Poon, A.S.Y. (2014). Wireless power transfer to deep-tissue microimplants. Proc. Natl. Acad. Sci. USA *111*, 7974–7979.

Huang, H., Michetti, C., Busnelli, M., Managò, F., Sannino, S., Scheggia, D., Giancardo, L., Sona, D., Murino, V., Chini, B., et al. (2014). Chronic and acute intranasal oxytocin produce divergent social effects in mice. Neuropsychopharmacology *39*, 1102–1114.

Jeong, J.W., McCall, J.G., Shin, G., Zhang, Y., Al-Hasani, R., Kim, M., Li, S., Sim, J.Y., Jang, K.I., Shi, Y., et al. (2015). Wireless Optofluidic Systems for Programmable In Vivo Pharmacology and Optogenetics. Cell *162*, 662–674.

Jong, T.R., Beiderbeck, D.I., and Neumann, I.D. (2014). Measuring virgin female aggression in the female intruder test (FIT): effects of oxytocin, estrous cycle, and anxiety. PLoS ONE *9*, e91701.

Jong, T.R., Menon, R., Bludau, A., Grund, T., Biermeier, V., Klampfl, S.M., Jurek, B., Bosch, O.J., Hellhammer, J., and Neumann, I.D. (2015). Salivary oxytocin concentrations in response to running, sexual self-stimulation, breastfeeding and the TSST: The Regensburg Oxytocin Challenge (ROC) study. Psychoneuroendocrinology *62*, 381–388.

Jurek, B., and Neumann, I.D. (2018). The Oxytocin Receptor: From Intracellular Signaling to Behavior. Physiol. Rev. *98*, 1805–1908.

Kagerbauer, S.M., Martin, J., Schuster, T., Blobner, M., Kochs, E.F., and Landgraf, R. (2013). Plasma oxytocin and vasopressin do not predict neuropeptide concentrations in human cerebrospinal fluid. J. Neuroendocrinol. *25*, 668–673.

Karpova, I.V., Mikheev, V.V., Marysheva, V.V., Bychkov, E.R., and Proshin, S.N. (2016). Oxytocin-Induced Changes in Monoamine Level in Symmetric Brain Structures of Isolated Aggressive C57Bl/6 Mice. Bull. Exp. Biol. Med. *160*, 605–609.

Kim, T.I., McCall, J.G., Jung, Y.H., Huang, X., Siuda, E.R., Li, Y., Song, J., Song, Y.M., Pao, H.A., Kim, R.-H., et al. (2013). Injectable, cellular-scale optoelectronics with applications for wireless optogenetics. Science *340*, 211–216.

Knobloch, H.S., Charlet, A., Hoffmann, L.C., Eliava, M., Khrulev, S., Cetin, A.H., Osten, P., Schwarz, M.K., Seeburg, P.H., Stoop, R., and Grinevich, V. (2012). Evoked axonal oxytocin release in the central amygdala attenuates fear response. Neuron *73*, 553–566.

Kondrakiewicz, K., Kostecki, M., Szadzińska, W., and Knapska, E. (2019). Ecological validity of social interaction tests in rats and mice. Genes Brain Behav. *18*, e12525.

Koolhaas, J.M., Coppens, C.M., de Boer, S.F., Buwalda, B., Meerlo, P., and Timmermans, P.J.A. (2013). The resident-intruder paradigm: a standardized test for aggression, violence and social stress. J. Vis. Exp. Published online July 4, 2013. https://doi.org/10.3791/4367.

Krakauer, J.W., Ghazanfar, A.A., Gomez-Marin, A., MacIver, M.A., and Poeppel, D. (2017). Neuroscience Needs Behavior: Correcting a Reductionist Bias. Neuron *93*, 480–490.

Lazzari, V.M., Becker, R.O., de Azevedo, M.S., Morris, M., Rigatto, K., Almeida, S., Lucion, A.B., and Giovenardi, M. (2013). Oxytocin modulates social interaction but is not essential for sexual behavior in male mice. Behav. Brain Res. *244*, 130–136.

Lee, H.J., Macbeth, A.H., Pagani, J.H., and Young, W.S., 3rd (2009). Oxytocin: the great facilitator of life. Prog. Neurobiol. *88*, 127–151.

Lee, H., Kim, D.W., Remedios, R., Anthony, T.E., Chang, A., Madisen, L., Zeng, H., and Anderson, D.J. (2014). Scalable control of mounting and attack by Esr1+ neurons in the ventromedial hypothalamus. Nature *509*, 627–632.

Lenth, R., Singmann, H., Love, J., Buerkner, P., and Herve, M. (2020). emmeans: Estimated Marginal Means, aka Least-Squares Means. https://cran.r-project.org/web/packages/emmeans/emmeans.pdf.

Lukas, M., Toth, I., Reber, S.O., Slattery, D.A., Veenema, A.H., and Neumann, I.D. (2011). The neuropeptide oxytocin facilitates pro-social behavior and prevents social avoidance in rats and mice. Neuropsychopharmacology *36*, 2159–2168.

Madisen, L., Zwingman, T.A., Sunkin, S.M., Oh, S.W., Zariwala, H.A., Gu, H., Ng, L.L., Palmiter, R.D., Hawrylycz, M.J., Jones, A.R., et al. (2010). A robust and high-throughput Cre reporting and characterization system for the whole mouse brain. Nat. Neurosci. *13*, 133–140.

Marroni, S.S., Nakano, F.N., Gati, C.D.C., Oliveira, J.A.C., Antunes-Rodrigues, J., and Garcia-Cairasco, N. (2007). Neuroanatomical and cellular substrates of hypergrooming induced by microinjection of oxytocin in central nucleus of amygdala, an experimental model of compulsive behavior. Mol. Psychiatry *12*, 1103–1117.

Mathis, A., Mamidanna, P., Cury, K.M., Abe, T., Murthy, V.N., Mathis, M.W., and Bethge, M. (2018). DeepLabCut: markerless pose estimation of user-defined body parts with deep learning. Nat. Neurosci. *21*, 1281–1289.

McCall, J.G., Kim, T.I., Shin, G., Huang, X., Jung, Y.H., Al-Hasani, R., Omenetto, F.G., Bruchas, M.R., and Rogers, J.A. (2013). Fabrication and application of flexible, multimodal light-emitting devices for wireless optogenetics. Nat. Protoc. *8*, 2413–2428.

Mickle, A.D., Won, S.M., Noh, K.N., Yoon, J., Meacham, K.W., Xue, Y., McIlvried, L.A., Copits, B.A., Samineni, V.K., Crawford, K.E., et al. (2019). A wireless closed-loop system for optogenetic peripheral neuromodulation. Nature *565*, 361–365.

Montgomery, K.L., Yeh, A.J., Ho, J.S., Tsao, V., Mohan Iyer, S., Grosenick, L., Ferenczi, E.A., Tanabe, Y., Deisseroth, K., Delp, S.L., and Poon, A.S. (2015). Wirelessly powered, fully internal optogenetics for brain, spinal and peripheral circuits in mice. Nat. Methods *12*, 969–974.

Ooi, Y.P., Weng, S.-J., Kossowsky, J., Gerger, H., and Sung, M. (2017). Oxytocin and Autism Spectrum Disorders: A Systematic Review and Meta-Analysis of Randomized Controlled Trials. Pharmacopsychiatry *50*, 5–13.

Pagani, J.H., Williams Avram, S.K., Cui, Z., Song, J., Mezey, É., Senerth, J.M., Baumann, M.H., and Young, W.S., 3rd (2015). Raphe serotonin neuron-specific oxytocin receptor knockout reduces aggression without affecting anxiety-like behavior in male mice only. Genes Brain Behav. *14*, 167–176.

Park, S.I., Shin, G., Banks, A., McCall, J.G., Siuda, E.R., Schmidt, M.J., Chung, H.U., Noh, K.N., Mun, J.G., Rhodes, J., et al. (2015a). Ultraminiaturized photovoltaic and radio frequency powered optoelectronic systems for wireless optogenetics. J. Neural Eng. *12*, 056002–56002.

Park, S.I., Brenner, D.S., Shin, G., Morgan, C.D., Copits, B.A., Chung, H.U., Pullen, M.Y., Noh, K.N., Davidson, S., Oh, S.J., et al. (2015b). Soft, stretchable, fully implantable miniaturized optoelectronic systems for wireless optogenetics. Nat. Biotechnol. *33*, 1280–1286.

Pedersen, C.A., Caldwell, J.D., Drago, F., Noonan, L.R., Peterson, G., Hood, L.E., and Prange, A.J., Jr. (1988). Grooming behavioral effects of oxytocin. Pharmacology, ontogeny, and comparisons with other nonapeptides. Ann. N Y Acad. Sci. *525*, 245–256.

Peters, S., Slattery, D.A., Uschold-Schmidt, N., Reber, S.O., and Neumann, I.D. (2014). Dose-dependent effects of chronic central infusion of oxytocin on anxiety, oxytocin receptor binding and stress-related parameters in mice. Psychoneuroendocrinology *42*, 225–236.

Peters, S.M., Pothuizen, H.H.J., and Spruijt, B.M. (2015). Ethological concepts enhance the translational value of animal models. Eur. J. Pharmacol. *759*, 42–50.

Qazi, R., Kim, C.Y., Byun, S.-H., and Jeong, J.-W. (2018). Microscale Inorganic LED Based Wireless Neural Systems for Chronic *in vivo* Optogenetics. Front. Neurosci. *12*, 764.

Qazi, R., Gomez, A.M., Castro, D.C., Zou, Z., Sim, J.Y., Xiong, Y., Abdo, J., Kim, C.Y., Anderson, A., Lohner, F., et al. (2019). Wireless optofluidic brain probes for chronic neuropharmacology and photostimulation. Nat. Biomed. Eng. *3*, 655–669.

Ragnauth, A.K., Devidze, N., Moy, V., Finley, K., Goodwillie, A., Kow, L.-M., Muglia, L.J., and Pfaff, D.W. (2005). Female oxytocin gene-knockout mice, in a semi-natural environment, display exaggerated aggressive behavior. Genes Brain Behav. *4*, 229–239.

Rossi, M.A., Go, V., Murphy, T., Fu, Q., Morizio, J., and Yin, H.H. (2015). A wirelessly controlled implantable LED system for deep brain optogenetic stimulation. Front. Integr. Nuerosci. *9*, 8.

Sala, M., Braida, D., Lentini, D., Busnelli, M., Bulgheroni, E., Capurro, V., Finardi, A., Donzelli, A., Pattini, L., Rubino, T., et al. (2011). Pharmacologic rescue of impaired cognitive flexibility, social deficits, increased aggression, and seizure susceptibility in oxytocin receptor null mice: a neurobehavioral model of autism. Biol. Psychiatry *69*, 875–882.

Shamay-Tsoory, S.G., and Abu-Akel, A. (2016). The Social Salience Hypothesis of Oxytocin. Biol. Psychiatry *79*, 194–202.

Shamay-Tsoory, S.G., Fischer, M., Dvash, J., Harari, H., Perach-Bloom, N., and Levkovitz, Y. (2009). Intranasal administration of oxytocin increases envy and schadenfreude (gloating). Biol. Psychiatry *66*, 864–870.

Shemesh, Y., Sztainberg, Y., Forkosh, O., Shlapobersky, T., Chen, A., and Schneidman, E. (2013). High-order social interactions in groups of mice. eLife *2*, e00759.

Shemesh, Y., Forkosh, O., Mahn, M., Anpilov, S., Sztainberg, Y., Manashirov, S., Shlapobersky, T., Elliott, E., Tabouy, L., Ezra, G., et al. (2016). Ucn3 and CRF-R2 in the medial amygdala regulate complex social dynamics. Nat. Neurosci. *19*, 1489–1496.

Shin, G., Gomez, A.M., Al-Hasani, R., Jeong, Y.R., Kim, J., Xie, Z., Banks, A., Lee, S.M., Han, S.Y., Yoo, C.J., et al. (2017). Flexible Near-Field Wireless Optoelectronics as Subdermal Implants for Broad Applications in Optogenetics. Neuron *93*, 509–521.

Steinman, M.Q., Duque-Wilckens, N., and Trainor, B.C. (2019). Complementary Neural Circuits for Divergent Effects of Oxytocin: Social Approach Versus Social Anxiety. Biol. Psychiatry *85*, 792–801.

Takayanagi, Y., Yoshida, M., Bielsky, I.F., Ross, H.E., Kawamata, M., Onaka, T., Yanagisawa, T., Kimura, T., Matzuk, M.M., Young, L.J., and Nishimori, K. (2005). Pervasive social deficits, but normal parturition, in oxytocin receptor-deficient mice. Proc. Natl. Acad. Sci. USA *102*, 16096–16101.

Tan, O., Musullulu, H., Raymond, J.S., Wilson, B., Langguth, M., and Bowen, M.T. (2019). Oxytocin and vasopressin inhibit hyper-aggressive behaviour in socially isolated mice. Neuropharmacology *156*, 107573.

van Anders, S.M., Goodson, J.L., and Kingsbury, M.A. (2013). Beyond "oxytocin = good": neural complexities and the flipside of social bonds. Arch. Sex. Behav. *42*, 1115–1118.

Warming, S., Costantino, N., Court, D.L., Jenkins, N.A., and Copeland, N.G. (2005). Simple and highly efficient BAC recombineering using galK selection. Nucleic Acids Res. *33*, e36.

Wentz, C.T., Bernstein, J.G., Monahan, P., Guerra, A., Rodriguez, A., and Boyden, E.S. (2011). A wirelessly powered and controlled device for optical neural control of freely-behaving animals. J. Neural Eng. *8*, 046021.

Williams, J.R., Insel, T.R., Harbaugh, C.R., and Carter, C.S. (1994). Oxytocin administered centrally facilitates formation of a partner preference in female prairie voles (Microtus ochrogaster). J. Neuroendocrinol. *6*, 247–250.

Winslow, J.T., Hearn, E.F., Ferguson, J., Young, L.J., Matzuk, M.M., and Insel, T.R. (2000). Infant vocalization, adult aggression, and fear behavior of an oxytocin null mutant mouse. Horm. Behav. *37*, 145–155.

Witt, D.M., Winslow, J.T., and Insel, T.R. (1992). Enhanced social interactions in rats following chronic, centrally infused oxytocin. Pharmacol. Biochem. Behav. *43*, 855–861.

Yizhar, O., Fenno, L.E., Prigge, M., Schneider, F., Davidson, T.J., O'Shea, D.J., Sohal, V.S., Goshen, I., Finkelstein, J., Paz, J.T., et al. (2011). Neocortical excitation/inhibition balance in information processing and social dysfunction. Nature *477*, 171–178.

Young, L.J., Winslow, J.T., Wang, Z., Gingrich, B., Guo, Q., Matzuk, M.M., and Insel, T.R. (1997). Gene targeting approaches to neuroendocrinology: oxytocin, maternal behavior, and affiliation. Horm. Behav. *31*, 221–231.

Zilkha, N., Sofer, Y., Beny, Y., and Kimchi, T. (2016). From classic ethology to modern neuroethology: overcoming the three biases in social behavior research. Curr. Opin. Neurobiol. *38*, 96–108.

Zoratto, F., Sbriccoli, M., Martinelli, A., Glennon, J.C., Macrì, S., and Laviola, G. (2018). Intranasal oxytocin administration promotes emotional contagion and reduces aggression in a mouse model of callousness. Neuropharmacology *143*, 250–267.

Please cite this article in press as: Anpilov et al., Wireless Optogenetic Stimulation of Oxytocin Neurons in a Semi-natural Setup Dynamically Elevates Both Pro-social and Agonistic Behaviors, Neuron (2020), https://doi.org/10.1016/j.neuron.2020.05.028

STAR★METHODS

KEY RESOURCES TABLE

REAGENT or RESOURCE	SOURCE	IDENTIFIER
Antibodies		
Chicken anti-GFP primary antibody	Aves labs inc.	RRID: AB_2307313
Goat anti-Chicken antibody (488 nm)	Abcam	RRID: AB_2636803
Guinea pig anti-OT antibody	Peninsula laboratories international	RRID: AB_518526
Goat anti-guinea pig antibody	ThermoFischer Scientific	RRID: AB_2534117
Rabbit anti-c-Fos antibody	Santa Cruz Biotechnology	RRID: AB_2106783
Goat anti-rabbit Alexa Fluor (594 nm)	ThermoFischer Scientific	RRID: AB_2813889
Bacterial and Virus Strains		
pAAV-Ef1a-DIO hChR2(C128S/D156A)-EYFP	https://web.stanford.edu/group/dlab/optogenetics/sequence_info.html#ssfo	Addgene_35503
Chemicals, Peptides, and Recombinant Proteins		
Quinine 90% powder	https://www.sigmaaldrich.com/catalog/product/aldrich/145904?lang=en&region=US	145904-10G
Oxytocin receptor antagonist	Tocris	L-368,899
Ornithine Vasotocin Analog (OVTA)	Perkin Elmer	NEX254050UC
Experimental Models: Organisms/Strains		
Ires-Cre-Oxt:Ires-Flp-Avp mice	This manuscript	N/A
Software and Algorithms		
IMARIS (9.5)	https://imaris.oxinst.com/	RRID: SCR_007370
Fiji	https://imagej.net/Fiji	RRID: SCR_002285
MATLAB R2019a	https://www.mathworks.com/products/matlab.html	RRID: SCR_001622
Pulse	https://www.heka.com/	N/A
Adobe Illustrator 23.1	https://www.adobe.com/	RRID: SCR_010279
"Social box" color-tracking and behavior analysis algorithm	https://bitbucket.org/Franck_Touboul/micegroupoptogenetics/src/master/	N/A
Other		
Fur marking dyes	"Tish & Snooky's" https://manicpanic.com/	HCR 11012; AMPLIFIED HCR11002; AMPLIFIED ACR-71031; HCR 11020
Multi-drain watch batteries	Energizer	ANSI/NEDA-1176SO, IEC-SR66
Light emitting diode (LED)	OSRAM	720-LBCP7PGZHX1
Magnetic reed-switch	Standex-Meder Electronics	KSK-1A80-1015
Implantable fiber optic cannula	Thorlabs	CFML14L02
Epoxy-Resin adhesive	https://www.mypolymers.com	N/A
Jet acrylic dental cement	http://www.langdental.com/pagenotfound/index	N/A
Miniature self-tapping screws	J.I. Morris	FF000CE094
Metabond adhesive resin kit	Parkell Inc.	S380

RESOURCE AVAILABILITY

Lead Contact

Further information and requests for resources and reagents should be directed to and will be fulfilled by the Lead Contact, Alon Chen (alon.chen@weizmann.ac.il or alon_chen@psych.mpg.de).

Please cite this article in press as: Anpilov et al., Wireless Optogenetic Stimulation of Oxytocin Neurons in a Semi-natural Setup Dynamically Elevates Both Pro-social and Agonistic Behaviors, Neuron (2020), https://doi.org/10.1016/j.neuron.2020.05.028

Materials Availability

Oxt::Cre mice are available upon request.

Data and Code Availability

The datasets and the code generated during this study are available at:
https://bitbucket.org/Franck_Touboul/micegroupoptogenetics/src/master/

EXPERIMENTAL MODEL AND SUBJECT DETAILS

Generation of Oxt::Cre (Ires-Cre-Oxt::Ires-Flp-Avp) mice

We used the bacterial artificial chromosome (BAC) recombineering techniques with the galK positive/negative selection system (Warming et al., 2005) to generate *Ires-Cre-Oxt::Ires-Flp-Avp* mice. In the same mice, to ensure eutopic expression of Cre-recombinase in OT-expressing neurons and Flp-recombinase in Avp-expressing neurons, we inserted *Ires-Cre* and *Ires-Flp* cassettes just downstream to the *Oxt* and *Avp* stop codons, respectively, using the RP23-100c5 BAC (see schematics here).

To prepare each of the recombineering targeting cassettes, we assembled the following 4 components for each cassette: [1] A-arm Oxt/Avp, which includes a homologous sequence for exon 2, intron 2, exon 3, and the stop codon of the *Oxt/Avp* gene, [2] the *Ires* coding sequence, [3] the *Cre/Flp* coding sequence, and [4] B-arm Oxt/Avp, which includes a homologous sequence for that located downstream of the *Oxt/Avp* gene. For this purpose, we used 8 sets of primers and carried out three rounds of PCR for each cassette (Table S2): In round 1, we carried out four PCR reactions per cassette, to amplify each of the 4 components separately. In round 2, we carried out two parallel PCR reactions per cassette, to ligate the A-arm *Oxt/Avp* with the *Ires* sequence and to ligate the *Cre/Flp* sequence with the B-arm *Oxt/Avp* sequence. In round 3, we carried out one PCR reaction per cassette, to ligate the PCR products from round 2 and complete the assembly of the 4 components of each cassette. For these ligations to take place during the PCR, subsets of the primers were designed to overlap with each other. Specifically, the sequence for primer Oxt-3 includes that for primer Oxt-2, the sequence for primer Oxt-5 includes that for primer Oxt-4, and the sequence for primer Oxt-7 includes that for primer Oxt-6. The same design was applied for the Avp cassette primer. Each cassette was cloned into the pGEM-T Easy vector (Promega) producing the pGEM-T Easy*:Oxt-Ires-Cre* and pGEM-T Easy*:Avp-Ires-Flp* vectors, which were then used as templates to amplify the recombineering targeting cassettes. The insertion of the *Ires-Cre* and *Ires-Flp* recombineering targeting cassettes into the precise location in the BAC was carried out via two consecutive steps: [1] to insert the *Oxt-Ires-Cre* recombineering targeting cassette into the BAC, [2] to insert the *Avp-Ires-Flp* recombineering targeting cassettes into the recombineered BAC already containing the *Oxt-Ires-Cre* cassette. Recombination was done following the protocol by Warming et al., 2005. Briefly, we used galK positive selection to insert a PCR-amplified *galK* cassette flanked by 45-50 bp homology arms to the insertion site in the BAC backbone, using the *pgalK* plasmid as a template and the Oxt-galK-F and 3′-Oxt-galK-R and the Avp-galK-F, and Avp galK-R primers to amplify the *galk* cassettes (Table S2). Next, we replaced the *galK* cassette using DOG counter-selection with a PCR amplified targeting cassettes flanked by similar 40-55 bp homology arms, using the Oxt-Ires-Cre-F and Oxt-Ires-Cre-R primers for the *Oxt-Ires-Cre* cassette, and the Avp-Ires-Flp-F and Avp-Ires-Flp-R primers for the *Avp-Ires-Flp* cassette (Table S2). The BAC was recombineered in SW102 cells. The direction of the inserted recombineering targeting cassettes was then determined by SrgAI digestion and separation of the digestion products by pulsed-field gel electrophoresis (PFGE). The recombined regions of the BAC were also sequence-verified. The recombined regions acquired two mutations: [1] a "TATG" sequence located just downstream of the *Oxt* gene stop codon and upstream of the *Ires* sequence was substituted by a "GTCA"; and [2] a "G" was substituted to "A" in the 288th base within the *Ires* sequence in the *Avp-Ires-Flp* cassette. None of the mutations had a deleterious effect, as reflected by normal Cre and Flp expression and activity in the *Oxt-Ires-Cre::Avp-Ires-Flp* mice.

To release the *loxp* sites located in the BAC backbone, we digested the *Oxt-Ires-Cre:Avp-Ires-Flp*-BAC with AscI. This digestion liberated a 16.4 kb fragment, as determined by PFGE, which contained the recombineered *Oxt* and *Avp* genes locus that was then isolated and used for embryonic stem cell targeting. Clones with confirmed homologous recombination were microinjected into CB6 blastocysts to create chimeric mice. Chimeric animals generated from blastocyst implantation were then bred for germline transmission of the altered *Oxt* and *Avp* gene locus and then backcrossed into C57/BL for 6 generations.

Animals

We used the transgenic *Oxt::Cre* male mice (congenic on C57BL/6 background; involves C57BL/6, FVB/N, ICR and unspecified strains). *Oxt::Cre*$^{+/-}$ males were mated with WT ICR females to obtain both *Oxt::Cre*$^{+/-}$ and *Oxt::Cre*$^{-/-}$ offspring. For the group experiment, male littermates were genotyped and separated into groups of 4 subjects of the same genotype within each group (6 groups of Cre^{+} and 5 groups of Cre^{-}) at weaning age (3 weeks). For immunohistochemical co-localization and *ex vivo* electrophysiological experiments, *Oxt::Cre*$^{+/-}$ mice crossed with the Ai9 reporter mouse line were used. For the RI paradigm, 5-week old C57BL/6 male juveniles were used as intruder conspecifics. All WT C57/BL6 and ICR mice were acquired from ENVIGO (Jerusalem, Israel). Throughout the experiments, the animals were maintained in a temperature-controlled room (22 ± 1°C) on a 12h:12h light–dark cycle (lights on at 22:00) in specific pathogen-free conditions. All experimental protocols were approved by the Institutional Animal Care and Use Committee (IACUC) of the Weizmann Institute of Science.

Please cite this article in press as: Anpilov et al., Wireless Optogenetic Stimulation of Oxytocin Neurons in a Semi-natural Setup Dynamically Elevates Both Pro-social and Agonistic Behaviors, Neuron (2020), https://doi.org/10.1016/j.neuron.2020.05.028

METHOD DETAILS

Fabrication of wireless optogenetic device

The device is comprised of two multi-drain watch batteries (377/376 1.55V, 0% Hg, SR626SW silver-oxide, Energizer), a light-emitting diode (Oslon SSL 80, blue light, 464-476 nm 'LB CP7P' LED, OSRAM), a reed-switch (Standex-Meder Electronics, KSK-1A80-1015) and an optic cannula (400 μm core implantable 5 mm long fiber optical cannula with 1.25 mm diameter, stainless steel ferrule, Thorlabs CFML14L02). The LED was attached to the optic cannula using a custom-made epoxy adhesive engineered to match the refractive index of the optic fiber (MyPolymers, Epoxy Resin EP-150). Next, the components were connected in series (Figures 1A and 1B). The device was then coated with jet-acrylic dental cement (Lang Dental Manufacturing Co., Wheeling, IL, USA) and brushed with quinine (Sigma-Aldrich, 145904-10G) to prevent other cage-mates from damaging it. On average, the total weight of the device amounts to ~1 gr without the dental cement.

Specific SSFO expression in PVN-OT neurons

Adeno-associated viral (AAV)-mediated gene delivery was used for heterologous Cre-dependent expression of SSFO in mice. To restrict expression of SSFO specifically to OT expressing cells, we expressed the double-floxed inverted open-reading-frame (DIO) AAV encoding SSFO and eYFP (pAAV-Ef1a-DIO hChR2(C128S/D156A)-EYFP; Addgene viral prep #35503-AAV1; Figure S1A) in *Oxt::Cre* transgenic mice.

Stereotaxic injections and mounting of the wireless optogenetic device

All experimental mice underwent stereotaxic injections with AAV1/2-Syn-DIO-SSFO-eYFP at the age of 10 weeks. Mice were mildly anesthetized with isoflurane. Corneas were protected from drying using eye gel (Viscotears liquid gel; Alcon). Mice were placed on a computer-guided stereotaxic instrument (Angle Two Stereotaxic Instrument, myNeurolab, Leica Microsystems Inc., Bannockburn IL, USA), which is fully integrated with the Franklin and Paxinos mouse brain atlas through a control panel. A midline incision was made across the top of the skull. After cleaning the periosteum, the vertical coordinates of bregma and lambda were measured to align in the same plane (level head). Viral vectors were delivered using a Hamilton syringe connected to a motorized nano-injector (350 nL with a rate of 50 nl/min). To allow diffusion of the solution into the brain tissue, the needle was left in place for an additional 10 min after the injection (coordinates relative to bregma: AP = −0.9 mm, ML = 0 mm, DV = −4.4 mm, based on a calibration study in this strain). The wireless optogenetic device was mounted following the injection during the same surgical operation. Prior to the insertion of the optogenetic device, a miniature, self-tapping screw was fixed on the skull (J.I Morris Company #303 stainless steel, FF000CE094). The device was lowered onto the head such that the tip of the optic fiber was located 0.1 mm above the injection site, and secured on the skull using a Metabond kit (Parkell Inc., Edgewood NY, USA) and Jet acrylic dental cement (Lang Dental Manufacturing Co., Wheeling IL, USA) anchoring to the inserted screw for better fixation. After the surgery, mice were given oral antibiotics (Enrofloxacin 5%, 0.6ml per 100 ml of drinking water) for 1 week. In the rare occasion of inflammation, mice were excluded from further research. Additionally, brain tissue damage was examined post-mortem and in most cases found to be as expected in cannulation experiments. In rare cases, where unusual tissue damage was observed in post-mortem IHC, mice were excluded from analysis.

Fur marking for video tracking

Ten days after surgery the fur of the mice was stained with semi-permanent hair dyes, then dried with a regular fan (low power and heat) for 3 min. After waking, mice were kept in separate boxes for 4 hours before reunion. Mice were introduced to the arena for tracking 5 days after fur staining. The dyes used were "Electric banana" (HCR 11012), Atomic Turquoise (AMPLIFIED HCR11002), Ultra Violet (AMPLIFIED ACR-71031) and Pillarbox Red (HCR 11020) from Tish & Snooky's (https://manicpanic.com; New York NY, USA). Mice were identified and tracked automatically according to their fur colors, which were learned from labeled data.

Light penetration in brain tissue

To estimate the distribution of light as a function of distance from the fiber tip, we used a slice of brain tissue placed on a thin diffusing layer revealing the 2-dimensional pattern of illumination at the bottom of the slice. This screen was imaged from below as the fiber was lowered through a gray matter portion of brain tissue. Light was delivered by a cannula adhered to an LED (both parts are identical to the ones used for the device). The LED and cannula were fixed to a computer-guided stereotaxic instrument (Angle Two Stereotaxic Instrument, myNeurolab, Leica Microsystems Inc., Bannockburn IL, USA) and the LED was connected to a power supply (EXTECH instruments, 382200 DC power supply) delivering 3.2 $mW \cdot mm^{-2}$ of blue light (468 nm) at the tip of the fiber. At each step, the fiber was lowered 50 μm and the 2-dimensional illumination pattern was recorded. A 3D map of the spread of blue light was reconstructed using the collected set of images using a custom-written MATLAB code.

Electrophysiology

Acute brain slice preparation

Acute brain slices were prepared from adult (12-14 weeks old) *Oxt::Cre* mice injected with AAV1/2-EF1α-DIO-SSFO-eYFP. Mice were anesthetized with isoflurane and perfused with carbogenated (95% O_2 / 5% CO_2) ice-cold slicing solution consisting of

(in mM): 2.5 KCl, 11 glucose, 234 sucrose, 26 $NaHCO_3$, 1.25 NaH_2PO_4, 10 $MgSO_4$, 2 $CaCl_2$; pH 7.2-7.4; 340 mOsm. After decapitation, the brain was rapidly removed from the cranial cavity and 300 μm thick coronal slices containing the PVN were prepared in carbogenated ice-cold slicing solution using a vibratome (HM650V; ThermoScientific). Afterward, slices were allowed to recover for 30 min at 34°C in carbogenated artificial cerebrospinal fluid (ACSF) containing (in mM): 125 NaCl, 2.5 KCl, 11 D-glucose, 25 $NaHCO_3$, 1.25 NaH_2PO_4, 1 $MgCl_2$, 2 $CaCl_2$; pH 7.2-7.4; 300 mOsm). Subsequently, slices were stored at room temperature (25°C) in carbogenated ACSF for at least 45 min.

Whole-cell patch-clamp recordings from hypothalamic slices

All experiments were carried out at 25°C. Slices were continuously perfused with carbogenated ACSF at a flow rate of 4-5 ml/min, in a submerged-type recording chamber. OT neurons of the PVN expressing the SSFO-eYFP were identified by epifluorescence microscopy. Afterward, the cell bodies of these neurons were visualized by infrared microscopy and the gradient contrast system. Somatic whole-cell patch-clamp recordings (seal resistance > 1 GΩ) were performed in bridge mode using a discontinuous single-electrode voltage-clamp amplifier (SEC-10L, npi electronics, Tamm, Germany). The current/potential was low-pass filtered at 3 kHz, digitized at 6.5 kHz via an ITC-16 interface board, and stored with the standard software Pulse 8.31 (HEKA Elektronik, Lambrecht / Pfalz, Germany). The patch-clamp electrodes (open-tip 5-7 MΩ) were pulled from borosilicate glass capillaries (Harvard Apparatus, Kent, UK) on a DMZ-Universal puller (Zeitz Instruments, Munich, Germany) and filled with a solution consisting on (in mM): 130 potassium gluconate, 5 NaCl, 2 $MgCl_2$, 5 D-glucose, 10 HEPES, 0.5 EGTA, 2 Mg-ATP, 0.3 Na-GTP, 20 phosphocreatine, pH 7.3 with KOH, osmolarity 305 mOsm (potentials were corrected for a liquid junction potential of 13 mV). The access resistance (R_a) was continuously monitored and recordings were terminated if R_a changed > 15%.

Electrophysiological measurements were carried out 5 min after reaching the whole-cell configuration. The input resistance was calculated from steady-state voltage responses upon negative current injections (1500 ms). The resting membrane potential (Vm) of SSFO-expressing neurons was 60.2 ± 1.5 mV. The light beam of a Sapphire 488 nm (75 mW max. output power) or Sapphire 561 nm (75 mW max. output power) laser (Coherent) was collimated into an optical fiber (BFL37-200, Thorlabs), which was coupled into the epifluorescence port of an Axioskop 2 FS microscope (Zeiss, Göttingen, Germany; Dine et al., 2016). The duration of the light pulses was regulated by means of a LS3ZM2 shutter and VCM-D shutter driver (Vincent Associates). Light intensities in the focus plane were measured using the PM100 system (Thorlabs). Before each experiment, a 20 s pulse of 561 nm light was applied to convert all of the SSFO channels to the dark state and prevent run-down of the photocurrents. The SSFO was activated by a 1 s pulse of 488 nm and deactivated by a 10 s pulse of 561 nm. In some experiments, only the blue light pulse was applied to activate the SSFO and the deactivation occurred naturally over a period of approximately 30 min. Offline analysis to determine the SSFO-induced ΔVm was performed using Pulse software.

Immunohistochemistry and microscopy

Animals were anesthetized with Pental (1.4 g per kg body weight, i.p.) and perfused transcardially with 100 ml of phosphate buffer solution (PBS) followed by 100 ml of 4% paraformaldehyde in borate buffer, pH 9.5. The brains were removed and post-fixed in 30% sucrose using the same fixative at 4°C, frozen and sectioned coronally at 40 μm thickness using a sliding microtome (Leica Microsystems GmbH, Wetzlar, Germany) and stored in PBS at 4°C until used. Brain slices were blocked for 1 hr with PBS containing 0.3% Triton and 20% normal horse serum to prevent nonspecific binding.

Images were captured using a confocal microscope (Zeiss LSM510 and LSM700) at 10x or 20x magnification. Image analysis was carried out using IMARIS (9.5) software. Fiji (http://www.Fiji.sc/) was used to pseudo-color images and add scale bars.

eYFP staining for verification of injection site

Coronal brain sections were incubated for 48 hr at 4°C with chicken anti-GFP antibody (1:400) as the primary antibody (Aves labs inc., RRID: AB_2307313), followed by 48 hr at 4°C with Alexa Fluor 488 nm goat anti-chicken antibody (1:300, Abcam, RRID: AB_2636803).

OT staining for evaluation of transgene penetrance

Coronal brain sections of *Oxt::Cre*$^{+/-}$|*Ai9*$^{+/-}$ mice (n = 5) were incubated for 48 hr at 4°C with guinea pig anti-OT antibody (1:400, Peninsula laboratories international, RRID: AB_518526), followed by 48 hr at 4°C with Alexa Fluor 488 nm goat anti-guinea pig antibody (1:200, ThermoFischer Scientific, RRID: AB_2534117). For each fluorescent marker, the percentage of neurons co-expressing both fluorescent markers out of total number of fluorescent neurons was calculated.

c-Fos and eYFP co-staining for evaluation of neuronal activation

3 weeks following stereotaxic injections of the AAV-SSFO vector (as described above), *Oxt::Cre*$^{+/-}$ mice either underwent photoactivation (manually for ~2 s using a magnet), or were handled without photoactivation. 90 min following this manipulation, mice were sacrificed and perfused for immunohistochemical detection of c-Fos in PVN-OT neurons. Rabbit anti-c-Fos (1:1000, Santa Cruz Biotechnology, RRID: AB_2106783) and chicken anti-GFP antibody (1:400, as above) were the primary antibodies, followed by Alexa Fluor 488 goat anti-chicken (1:300, as above) and Alexa Fluor 594 goat anti-rabbit as secondary antibody (1:300, Life Technologies, RRID: AB_2813889).

OT levels in plasma

For measurement of baseline plasma levels of OT, operated mice (*Oxt::Cre*$^{+/-}$ and *Oxt::Cre*$^{-/-}$) were handled and, exactly 3 min later, subjected to submandibular blood collection under mild isoflurane anesthesia. For post-activation plasma OT measurement, 2 weeks

later, at the same stage of the diurnal cycle, the procedure was repeated, but 3 min following actual activation of the mounted devices rather than simple handling. To exclude exhaustion of the OT neurons or depletion of neuropeptide content, another set of operated mice (*Oxt::Cre*$^{+/-}$ and *Oxt::Cre*$^{-/-}$) were subjected to a regime of photoactivations similar to the main experiments (2 s long light pulses every 2 hr during the dark phase of the day, summing up to five activations per day). For baseline measurements, mice were handled instead of their devices being activated. In both cases, blood was collected as described above, 3 min following the last activation/handling. Plasma was extracted and OT levels were measured using an extremely sensitive and specific RIA kit (RIAgnosis, Sinzing, Germany) (Jong et al., 2015; Kagerbauer et al., 2013).

Receptor Autoradiography

Brains were coronally sectioned at 16 μm thickness and mounted on slides. The receptor autoradiography procedure was performed according to Young et al., 1997 using a linear OT receptor antagonist [125I]-d(CH2)5[Tyr(Me)2-Tyr-Nh2]9-OVT (Perkin Elmer, USA) as a tracer. Briefly, the slides were thawed and dried at room temperature followed by a short fixation in paraformaldehyde (0.1%). The slides were washed twice in 50 mM Tris (pH 7.4), exposed to tracer buffer (50 pM tracer, 50 mM Tris, 10 mM MgCl2, 0.01% BSA) for 60 min, and washed 4 times in Tris þ 10 mM MgCl2. The slides were then shortly dipped in pure water and dried at room temperature overnight. On the following day, the slides were exposed to Biomax MR films for 6 days (Kodak, Cedex, France). The films were scanned using an EPSON Perfection V800 Scanner (Epson, Germany). The optical density of OTR binding was measured using Fiji. Receptor density was calculated per mouse by taking the mean of bilateral measurements of 6 to 12 brain sections per region of interest after subtraction of tissue background.

Social arenas

Mouse behavior was studied in a specialized arena designed for automated tracking of individual and group behavior (Figure 1C). Each arena housed a group of 4 male mice of the same genotype (either Cre^{+} or Cre^{-}) at the age of 13 weeks. The arena consisted of an open 70 × 50 × 50 cm box and included the following objects: Z-shaped wall, a water dispenser, two feeders, an open shelter, a large nest, an elevated block, and two elevated ramps. During the light phase (12 h) arenas were illuminated with 200 lux and during the dark phase (12 h) with a 2 lux diffuse light provided by two True-Light bulbs (fluorescent lamps, 23W E27 5023 True-Light International GmbH) placed under the arenas. The mice were recorded only in the dark phase using a digital color-sensitive camera (Manta G-235C, Allied-Vision) which was placed 1 m above the arena. Mouse trajectories were automatically detected offline using custom software in MATLAB (R2019a, MathWorks, Natick, MA, USA).

Photoactivation in social arenas

Dark-phase activity of the mice was recorded for 6 consecutive days. During days 5 and 6 of the experiment, the optogenetic device of each group member was remotely activated for approximately 2 s, roughly every 2 hr, resulting overall in 5 activations per dark phase per mouse. For the activation of the wireless devices in the arena, 2 electromagnets (ZYE1-P Round Holding Magnets, CNZYEM, China) were installed on a short, tunnel-like structure that connects between the arena and 'feeder 1'. Thus, activation of the implanted devices was possible upon the mice entering the feeder. The electromagnets were controlled by a custom-written MATLAB code, using a digital USB I/O module (NI USB-6501, (24-ch, 8.5 mA), National Instruments). Photoactivation events were monitored in the video recording.

Identification and classification of interactions between mice

We automatically identified and classified interactions between mice as events in which the distance between a pair of mice (d) was shorter than 10 cm. We then used the movement direction of one mouse relative to another mouse (θ) to identify the nature of the contact for either of the mice. If for mouse A, the projection of the direction of its movement relative to mouse B was small enough ($|\tan(\theta)\cdot 2d| < \Theta_1, for -(\pi/2) < \theta < (\pi/2)$) then it was considered as moving toward B; if $|\tan(\theta)\cdot 2d| < \Theta_2$ $for (\pi/2) < \theta < (3/2)\pi$ it was moving away from it; otherwise it was assumed idle with respect to the other mouse (Θ_1 and $\Theta_2$were found by optimization).

As described in Shemesh et al., 2016, to classify aggressive and non-aggressive contacts, we first used a hidden Markov model to identify post-contact behaviors in which mouse A was moving toward B, and B was moving away from A (i.e., A was following B). We then used 500 manually labeled events to learn statistical classifiers of aggressive and non-aggressive post-contact behavior. For each event, we estimated a range of parameters, including individual and relative speed, distance, etc., and optimized a quadratic discriminant classifier, a k-nearest neighbor algorithm based on these parameters, and a decision-tree classifier that used these parameters at each tree intersection. We found that for a test set of 1000 events, none of these classifiers were accurate enough individually, but that a combined approach in which we labeled an event as 'aggressive' if any of the classifiers labeled it as such – gave ~80% detection with 0.5% false alarms.

Quantification of close social investigation among conspecifics

Since our previously-described automated tracking system is currently unable to automatically recognize specific body parts, this system was only used to select from each video 150 frames in which exactly 2 mice were in close contact (< 3.5 cm between their body ends) in the open area. From each video 150 such frames were randomly sampled (11 groups × 3 days × 150 frames = 4950 frames). These frames were then manually classified by human observers, who were blind to the genotype of the group, as either 'face-to-face' investigation, 'face-to-back' investigation, or 'others' (e.g., tail-to-tail contact). The ratio between face-to-face and face-to-back investigations was then calculated only for these 2 behaviors (i.e., disregarding other contacts).

Please cite this article in press as: Anpilov et al., Wireless Optogenetic Stimulation of Oxytocin Neurons in a Semi-natural Setup Dynamically Elevates Both Pro-social and Agonistic Behaviors, Neuron (2020), https://doi.org/10.1016/j.neuron.2020.05.028

Pairwise automatic behavioral readouts

- Contact rate: Number of contacts the mouse had. A contact is defined as conspecifics being less than 10 cm apart while both are outside the nest (1/hour).
- Time in contact: Fraction of time that a mouse is in contact with other mice while outside the nest (1/hour).
- Median contact duration: Median duration of contacts. The contact duration does not include the times when the mouse approached, moved away from, or chased a conspecific (seconds).
- Chase rate: Chases are interactions that ended with the mouse pursuing a conspecific in an aggressive manner. Aggressiveness was determined using a classifier that was trained on 500 manually scored samples (1/hour).
- Escape rate: Number of time that the mouse was aggressively chased by a conspecific (1/hour).
- Chase rate (non-aggressive): Number of times the mouse has chased a conspecific at the end of a contact in a non-aggressive way, as determined by the classifier (1/hour).
- Escape rate (non-aggressive): Number of times the mouse was chased by a conspecific at the end of a contact in a non-aggressive way, as determined by the classifier (1/hour).
- Approach rate: An approach is a directed movement of the mouse toward a conspecific that ends in contact. Not all interactions necessarily start with an approach, while others might start mutually with conspecifics approaching each other (1/hour).
- Approach rate (per mice out): number of approach events normalized by the time being outside the nest with at least one more conspecific (1/hour).
- Rate of being approached: Number of times the mouse was approached by a conspecific (1/hour).
- Alone outside: Fraction of time the mouse is outside the nest while all other mice are in the nest (au).

Individual automatic behavioral readouts

- Time outside: Fraction of time that the mouse spends outside of the nest (% of total).
- Rate of visits outside: The rate at which the mouse exits the nest (1/hour).
- ROI exploration: Quantifies the amount of exploration the mouse is doing. Measured as the entropy of the probability of being in each of the 11 regions-of-interest (ROIs) (excluding the nest). Mice that spend the same amount of time in all regions will get the highest score, while mice that spend all their time in a single ROI will be scored zero. When normalized to the time outside, the computation of the entropy differed also by ignoring the probability of being inside the nest (bits/hour).
- Distance: The total distance traveled by the mouse while outside the nest. To smooth the tracking, the mice locations were sampled once every second (m).
- Median speed: Median speed while outside the nest. To smooth the computation of the speed, the mice locations were sampled once every second (m/sec).
- Tangential velocity: The tangential component of the speed, or the part of speed perpendicular to the previous direction of movement (m/sec).
- Angular velocity: The rate of change in the direction of the mouse (rad/sec).
- Food or water: Time spent next to the feeders or water bottles (au).
- Elevated area: Time spent on an elevated object in the arena: ramps or block (au).
- Distance from walls: Average distance from the walls while in the open area (cm).

Self-grooming

Trained observers, blind to the genotype of the mice, observed the recorded movies for a period of 5 min following each optogenetic activation. Only activations that could be detected by observing the movie were chosen. The onset and the duration of each grooming event within the observed 5 min period were scored. For self-grooming events at baseline (experimental day 4), on which no activations were made, visits to 'feeder 1' were randomly sampled and leaving the feeder was chosen as a reference time-point for the 5 min period of observation.

Automated feeders

During the recording, access to food was manipulated by automatic feeders controlled by custom-written software in MATLAB, such that food was accessible in a pseudo-random manner cumulatively for 5 hr per day. This time frame was chosen based on data from early studies in the arenas that showed mice would spend on average 1-2 hr in the feeder zones when food was freely available (Shemesh et al., 2013). The gate of each feeder was connected to a servo motor (Hitec HS-422 deluxe, Part No: 31422S). The servo was controlled by a digital 'National Instruments' device (USB-6501, 24-Channel Digital I/O, programmable 5 V, TTL or 3.3 V, 8.5 mA and NI-DAQ Drivers).

Resident-intruder

Cre^+ and Cre^- male mice underwent stereotaxic virus injection and device implantation in a single surgical operation at the age of 10 week. Following recovery, the males were housed in a large cage (37 × 21 × 24 cm). To improve the establishment of territory, a female was introduced to the cages for 6 days and the bedding was not changed (Koolhaas et al., 2013). On day 7 the females were removed from the cages, and the wireless device of the males were activated using a magnet every 2 hr during the dark phase, between 10:00-18:00 (a total of 5 activations). On day 8, the devices were activated at the beginning of the dark phase, then followed

with an i.p. injection of either the OTR antagonist L-368,899 (Cre^+ mice only) or saline (both Cre^+ and Cre^- mice) 90 min later. 30 min following injection, the devices were activated again right before the introduction of the intruder conspecific. Intruders were unfamiliar 5-week old C57/BL6 male juveniles. Mice were allowed to roam freely for 10 min, unless testing had to be stopped due to severe aggression shown by the resident. For behavioral scoring, the interactions were recorded using an infra-red (IR) camera (Basler ace acA1300-60 gm, Basler AG, Germany), and an IR illuminator was used to illuminate the cage. Behavioral scoring was performed by a trained observer blind to the treatment using the 'Solomon Coder' freeware (https://solomon.andraspeter.com/). Attacking, biting, bite attempts, offensive upright position and chasing were grouped as 'aggressive behavior'. Mounting, thrust, tail rattling and aggressive allo-grooming were grouped as threat behavior. In addition to the above behaviors, self-grooming, rearing, face sniffing, trunk sniffing and ano-genital sniffing were scored (Figure S2C). For quantification of locomotion, the resident animals were tracked using DeepLabCut (Mathis et al., 2018). Subsequent data analysis was performed using a self-written MATLAB code.

QUANTIFICATION AND STATISTICAL ANALYSIS

Multi-variate separation was calculated as Euclidean distance between the centroids of Cre^+ and Cre^- mice in 21 dimensions of the automatically collected behavioral readouts. Statistical inference was based on comparison to a null distribution comprised of Euclidean distances corresponding to 1×10^5 randomly reshuffled partitions.

PCA was performed separately on the Z-scores of the difference values of the 2 activation days from baseline (experimental day 4). To determine the percentage of variance explained by each PC in a random dataset, explained variance was independently calculated from one million randomly reshuffled versions of the original dataset. Specifically, reshuffled datasets were created by independently reshuffling the variables within each observation.

For inferential comparisons between two samples, Monte Carlo permutation test of means (1×10^7 permutations) was carried out, except for data of electrophysiological recordings, plasma OT levels and grooming related measurements (group experiment), where exact paired permutations test was applied. In electrophysiological data, as well as grooming-related measurements in the group experiment, a specific direction of the response was expected based on previous evidence, therefore a one-tailed approach was employed.

Kruskal-Wallis one-way analysis of variance with Dunn & Sidak's post hoc test were used for the RI experiment. Non-parametric tests were employed, as data did not fulfil criteria for parametric testing (normality of residuals and equal variances between experimental groups).

For hierarchical rank as predictor of behavior, Pearson's correlation coefficient was computed. Alpha level of significance was adjusted using the Bonferroni method.

All above analyses were performed using MATLAB.

For temporal analysis of behavior before and after photoactivation, approach and chase events were collected for each mouse in a time window of 1 hr preceding activation and 1 hr following, for all activations except the first one of each activation day. This time window was divided into 3-min bins and for each mouse the average count of behavioral events per bin was calculated from the different activations of each day. These data were then analyzed by fitting a linear mixed effects model with Genotype*Time as the fixed effects, and Mouse nested within Group as the random effects. Significance of the fixed effects was assessed by running analysis of variance on the model. Where appropriate, post hoc Tukey comparisons of estimated marginal means were done between genotypes for each time point. Analyses were performed in R (https://www.r-project.org/) using the "lme4" (Bates et al., 2015) and "emmeans" (Lenth et al. 2020) packages.

The computation of IDs was performed as described in Forkosh et al., 2019. The changes in the first 4 IDs from baseline (day 4) to each day of activation were then computed for each mouse. The delta values were then analyzed by fitting a linear mixed effects model with Genotype*Day as the fixed effects, and Mouse nested within Group as the random effects. Significance testing was conducted in R as described above.